Department of Industrial Engineering

PhD School in Industrial Engineering

PhD in Energy Engineering and
Innovative Industrial Technologies

XXVII cycle (2012-2014)

Development of numerical methods for low pressure turbine tone noise analysis

Scientific disciplinary sector: ING-IND/09

PhD student: Ing. Ettore Di Grazia

Supervisor: Prof. Andrea Arnone

Co-supervisor: Dr. Lorenzo Pinelli

Co-supervisor: Dr. Torzo Davide

Coordinator: Prof. Maurizio De Lucia

Florence, December 2014

Silence is a source of great strength
Lao Tze

Dedicated to my parents

Contents

List of Figures

List of Tables

Nomenclature

a	speed of sound
c	absolute velocity
$\underline{F}_{x,\theta,r}$	cylindrical flux functions
G	angular pitch
$\vec{I}_a$	acoustic intensity
j	imaginary unit ($j^2 = -1$)
k_x	axial wave number
k_y	circumferential wave number
ℓ, m	circumferential order
M_T	tangential wave Mach number
M_x	axial Mach number
M_y	circumferential Mach number
N	Blade number
p	pressure
s	specific entropy
T	temperature

t	time coordinate
$\underline{\mathscr{U}}$	radial mode shape
u	axial velocity component
v	circumferential velocity component
W_{ac}	sound power
x	axial coordinate
x, θ, r	cylindrical coordinates
x, y, z	orthogonal Cartesian coordinates

Greek:

Ω	rotational speed
ω	frequency of the wave
ϕ	phase of the wave
ϱ	density
Σ	section of the annular duct
θ	angular coordinate

Subscripts and undersigns:

$_d$	downstream running acoustic wave
$_u$	upstream running acoustic wave
$_\xi$	entropy wave
$_s$	entropy wave
$_{\mathrm{ref}}$	reference quantities
$_{\mathrm{rsm}}$	root mean square

Acronyms:

BPF	Blade Passing Frequency
CAA	Computational Aeroacoustics
CFD	Computational Fluid Dynamics
DFT	Discrete Fourier Trasnform
DIEF	Department of Industrial Engineering of Florence
EPNdB	Effective Perceived Noise in decibel
ICAO	International Civil Aviation Organization
LEE	Linearized Euler Equations
LPT	Low-Pressure Turbine
PWL	sound PoWer Level
RMA	Radial Mode Analysis
SPL	Sound Pressure Level
TNT	Tone Noise Tool
TRF	Turbine Rear Frame

Superscripts and oversigns:

$\bar{}$	averaged quantities
$'$	perturbed quantities
$\vec{}$	vector quantities

Introduction

One of the major concerns in the urban areas surrounding airports is the noise pollution caused by the acoustic emissions coming from aircraft operations. It has been demonstrated that a continuous and prolonged exposure to noise pollution, not only results in a lower quality of life, but has harmful effects on human health as well. Definitely, noise may be the cause of psychological disorders, such as insomnia, anxiety, aggressiveness, and physiological disturbances, such as hearing impairment, hypertension and ischemic heart diseases. For these reasons, since the 1960s, when turbojet engines spread in the aviation industry, regulations on aircraft noise emissions have been introduced. Afterwards, due to the continuous growth in air traffic, these legislations have become more and more restrictive. This led to the introduction of the noise certification process for commercial aircrafts at the operating points critical in terms of noise perceived on the ground.

Due to the introduction of noise regulations, the goal of reducing the acoustic emissions produced by aircrafts has been a constant challenge for aeronautical industry and engine designers continuously strives hard to to develop quieter components. In this context experimental and numerical investigations on noise generation and propagation mechanisms have become a main research field for aeronautical manufacturers. Such studies are aimed at gaining a deeper insight on the physical phenomena in order to develop effective low noise strategy.

In particular, well-calibrated and reliable numerical tools for noise prediction can be used within the engine design loop allowing the evaluation of the acoustic emissions caused by each component before it is tested in a demonstrator. As a consequence, these tools are of great importance in the reduction of aircraft noise.

Aeroacoustic simulations within an engine environment can be performed by means of different techniques, ranging from analytical models to 3D numerical solvers: fast and robust methods have primary importance at the beginning of the design loop, when it is essential to gain a general understanding of the effect of primary design parameters on the noise emissions. On the other hand, three-dimensional aeroacoustic solvers, more accurate and reliable, are able to to provide detailed knowledge of the acoustic phenomena during the advanced design verifications.

Aircrafts acoustic emissions can be divided into either external and internal noise. The former contribution arises from the interaction between the airflow and the aircraft itself (fuselage, wings, control surfaces, etc...), the latter instead is generated inside the engines as a result of various mechanisms and then radiates outside. At the dawn of civil aviation, the most critical noise source was the exhaust jet, but with the introduction of modern high-bypass ratio turbofan engines jet noise has been strongly reduced. Also fan noise has been drastically lowered over the years taking advantage of low-noise design criteria and acoustic treatments in the bypass duct. Hence, the other engine noise sources, such as the low-pressure turbine (LPT), have become significant in the overall aircraft emissions, first and foremost at some critical operating conditions. For this reason, nowadays a wide range of components need to be investigated during the engine design in order to apply low-noise criteria required to meet the increasingly restrictive noise regulations.

In this context, the main topic of this PhD thesis is the development of two different methods to be used when evaluating

the tone noise emissions of low pressure turbines. The first one is a two-dimensional model that computes the transmission of an acoustic wave across a blade row. This method has been included in a preliminary noise prediction procedure capable of quickly estimating the noise emissions of a multistage turbine. The second method allow the extraction of the acoustic waves from a 3D unsteady CFD solution obtained by Traf code. Traf code is commonly used to perform URANS simulations of a pair of neighbour blade rows. During this PhD activity, a post processing technique of the unsteady solution, based on the discrete Fourier transform, has been implemented in order to extract the acoustic components from the time depending solution at each BPF. Finally, after the DFT in time domain, tone noise levels can be calculated in terms of SPL and PWL values by means of radial mode analysis. The key aspects of this procedure are the capability to provide detailed results in terms of acoustic emissions for rotor/stator interactions within the pair of rows with a single simulation and to account for non-linear aeroacoustic effects, which can be relevant in modern low-pressure turbine environments (high pressure ratio, low axial spacing).

The validation of these methods has been carried out by comparing their results both with the results of simulations coming from a previously validated approach based on Lars code and acoustic experimental data measured at a cold-flow rig.

Finally, although these methods have been developed specifically for low-pressure turbines, they can be actually used in any axial turbo-machinery environment where rotor-stator interactions are relevant sources in the overall emissions.

Chapter 1

Aircraft noise issues

Since the dawn of commercial aviation, aircraft noise pollution has become a major environmental concern. The aim of this chapter is to introduce this issue, with particular attention on the human reaction to noise exposure and on the regulations proposed to deal with this problem. Finally, the most critical aircraft noise sources will be described together with the low-noise design criteria which have been developed over the years to abate sound levels.

1.1 Noise and its effects on people

A sound is the perception of a pressure fluctuation which can be generated by a wide range of physical phenomena and then propagates through a medium, usually the atmosphere, up to our auditory system. Human hearing can sense sounds with frequencies between 20 Hz and 20000 Hz; acoustic perturbations below and above those limits are called infrasound and ultrasound respectively. Noise, in turn, is defined as a sound that produces adverse effects, like harming, disturbing, or annoying people. Aircrafts are indeed one of the major noise source in our society and the noise coming from their

engines affects a large number of people living in the airports neighbourhoods and under landing or departing routes.

Figure 1.1: A Qantas Boeing 747 passing very close to house roofs in proximity of Heathrow airport

Since sound exposure effects are usually transitory and rarely fatal for human health, for a long time, noise has been wrongly considered a minor concern compared to other king of pollution, such as air or water contamination. Nevertheless, many negative effects can be caused by noise exposure, including hearing impairment, task performance degradation, sleep disturbances and general feeling of annoyance. Research studies indicate that also non auditory long-term health problems might result from excessive noise exposure, in particular cardiovascular diseases and hypertension. Such pathologies sometimes occur also in absence of detectable hearing loss.

The side effects of noise affliction primarily depend on sound intensity, being the amplitude of the pressure pertur-

bation. This quantity is measured in decibel (dB) using the Sound Pressure Level (SPL), which is defined as the decimal logarithm of the ratio between the root mean square of the wave amplitude and the nominal limit of human hearing threshold, that is 20 μPa in absence of auditory disfunctions:

$$SPL = 20 \log \left(\frac{p_{\text{snd}}}{p_{\text{ref}}} \right)$$

By means of the SPL value different sounds can be quantified and compared, allowing the evaluation of the noise pollution impact on people in an impartial manner, excluding social, physical or psychological factors. The limit of comfortable

Source of sound	SPL
Jet engine (30 m)	150 dB
Rifle shot (1 m)	140 dB
Threshold of pain	125 dB
Accelerating motorcycle (5m)	110 dB
Car horn (5 m)	100 dB
Hearing damage threshold	85 dB
Busy traffic (5 m)	80 dB
Vacuum cleaner (1 m)	70 dB
Normal conversation (1m)	60 dB
Quiet urban area at daytime	50 dB
Quiet urban area at nighttime	40 dB
Quiet library	30 dB
Clock ticking (3 m)	20 dB
Human breathing (3 m)	10 dB
Human threshold (good ears)	0 dB

Table 1.1: Approximate intensity of common sounds

hearing is commonly considered 65 dB; around 85 dB hearing damages begin in case the sound exposure is prolonged (8 hours) and over 90 dB hearing protections become mandatory

in working environments. Human threshold of pain is located at 125 dB: sounds at or above this limit cause immediate damage for the auditory system.

Also the distance from the source is essential, since radiating waves decay while propagating due to geometrical dispersion and air absorption. The former phenomenon consists in the acoustic power spreading due to wavefront expansion: it is independent of frequency and occurs in all sound radiation situations. Typical values of geometrical sound drops are around 6 dB and 3 dB per doubling of distance for spherical and cylindrical wavefronts respectively. The second mechanism dissipates acoustic energy by means of molecular relaxation and viscous effects, the first being the most relevant. Their effect depends on air temperature and humidity, and increases at higher frequencies. For this reason, sounds above 10 kHz have a little impact on the overall loudness.

Finally, the definition of a standard quantity to measure the harmfulness of noises must take into account also the physiological response of human auditory system to different sound frequencies: this response is not uniform since higher sensitivity occurs in the $2-4$kHz range. For this reason, it was introduced the Effective Perceived Noise in decibel (EPNdB), a quantity that evaluates noise effects on people taking into account the human response to both intensity and spectral shape of sounds.

1.2 The problem of aircraft noise

The advent of flying machines was one of the biggest technological revolutions occurred during the last century which deeply affected the evolution of human society. Obviously, the first applications were in the military field, but after only a few decades it spreads to civil transport as well. Since the conclusion of World War II, we have seen a constant development of civil aviation, supported by a constant growth in the air traffic. With the increase in flight length, height and speed,

indeed, farther destinations could be reached in shorter time and to a lower cost: for this reason, aircrafts have become one of the most important pillar in our transportation strategies. This is particularly true in the most developed nations where air transportation plays a crucial role in the quality of life of million of people that every day rely on flying to fulfill every kind of business.

Figure 1.2: Boeing 707: one of the first aircraft equipped with jet engines [image courtesy John Travolta, 2011]

However, flight technology has also introduced some environmental issues that have not been solved yet. In particular, with the spread of jet engines in the early 1960s, civil aviation finally took place (mainly due to the success of Boeing 707 in Figure 1.2 and Douglas DC-8), but the noise generated by exhaust gases became the loudest sources of noise in the community. In the meanwhile, as a consequence of the continuous growth in jet air traffic, noise emissions have become more and more frequent throughout a day, turning out to be

a serious downside for people living or working near airports and under flight paths (see Figure 1.3).

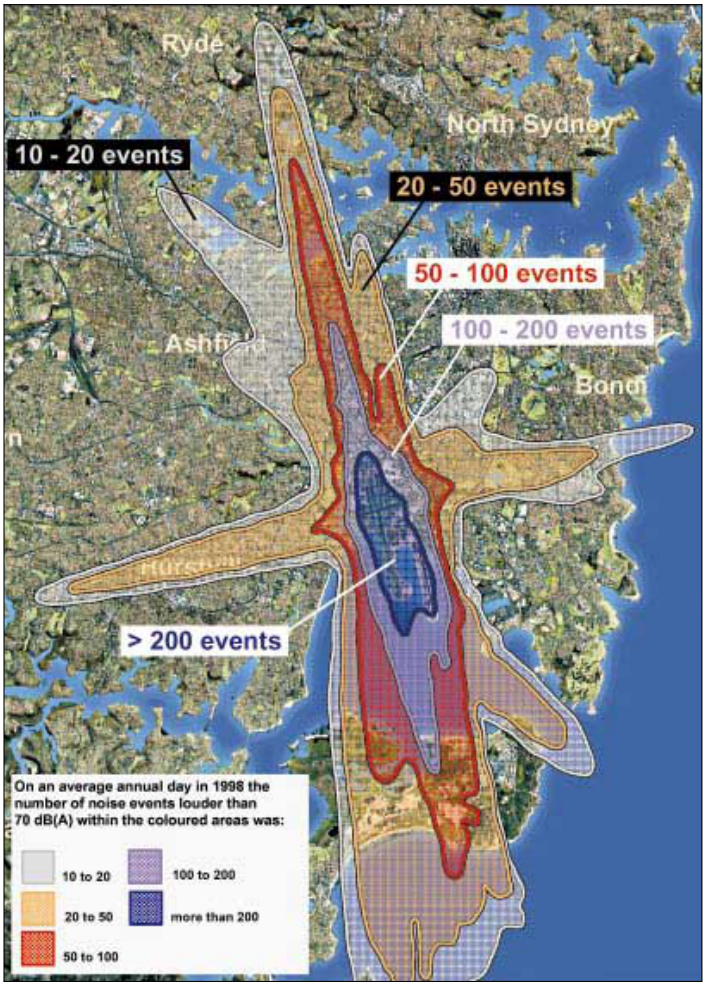

Figure 1.3: Noise contours around Sydney airport [10]

As a result, local administrations have started to establish legislations in order to control and limit aircraft noise. By the mid-1960s also central governments began a discussion about noise pollution near airports and, in the early 1970s, the idea of noise certification of aircraft finally took place. This happened in conjunction with the spread of the second generation of turbofan engines, which provided much higher performance, both in terms of efficiency and noise emissions.

The concept of noise certification is meant to ensure that manufacturers incorporate all the noise reduction technology available into their aircraft designs, providing effective reductions in the airports neighbours. Therefore, the effective noise levels of new aircrafts must be measured and assessed against given limits, which have been strongly strengthened since the 1970s. Meeting these requirements is mandatory to allow an aircraft to enter in commercial service and operate.

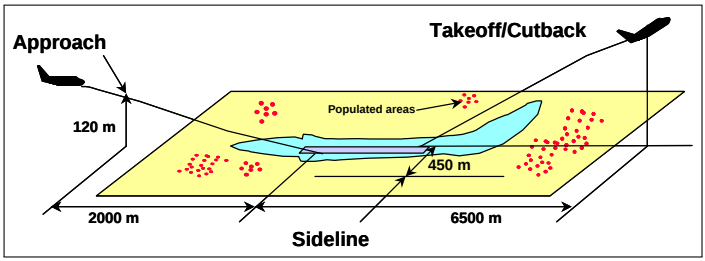

Figure 1.4: Noise certification operating points

Experimental procedures to evaluate the effective acoustic emissions have been delined by International Civil Aviation Organization (ICAO), a specialized agency of the United Nations which Member States refer when developing their national civil aviation regulations. Noise levels are measured with several microphones settled on the ground directly under the flight path or to the side of the track at three operating points: Approach, Cutback and Sideline [24] (see Figure 1.4).

A significant reduction in aircraft acoustic emissions (that today are more than 20 dB lower than those of the first generation of jets, as shown in Figure 1.5), has already been achieved over the last decades through the development of high bypass-ratio turbofan, liner technology and turbomachinery low-noise technologies. However, due to the constant reduction of al-

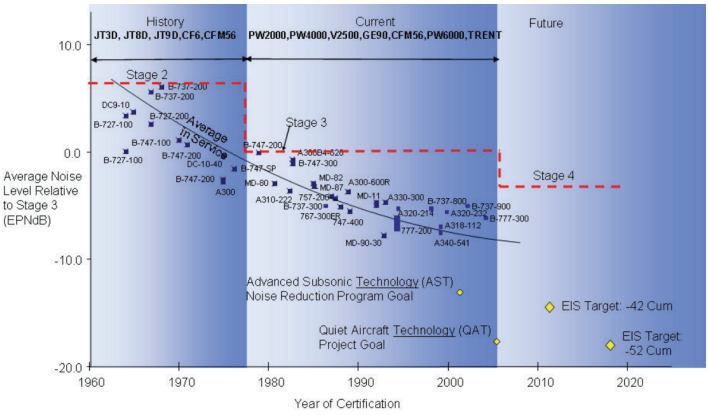

Figure 1.5: Progress in aircraft noise reduction [23]

lowed noise levels, manufacturers are continuously compelled to improve the acoustic performances of their aircrafts, that otherwise would not be certified. Therefore, to address the challenge of quieter flights, a great deal of efforts are being made to gain a deeper knowledge of the physical phenomena behind aircraft noise emissions in order to continuously improve low-noise noise technology.

Obviously, this is a very challenging task, not only for the different working conditions when the aircraft flies near the ground, but also because aerodynamic efficiency and weight reduction requirements are often achieved through solutions that are in contrast with low-noise criteria.

1.3 Aircraft noise sources

As shown in Figure 1.6, the overall acoustic emissions of an aircraft arise from a combination of a complex set of different sources. These sources can be classified as either external noise, gathering the various aeroacoustic phenomena taking place around the plane body, and internal noise, that generates and propagates inside the engine through different mechanisms and afterwords radiates outside. Hence, all the

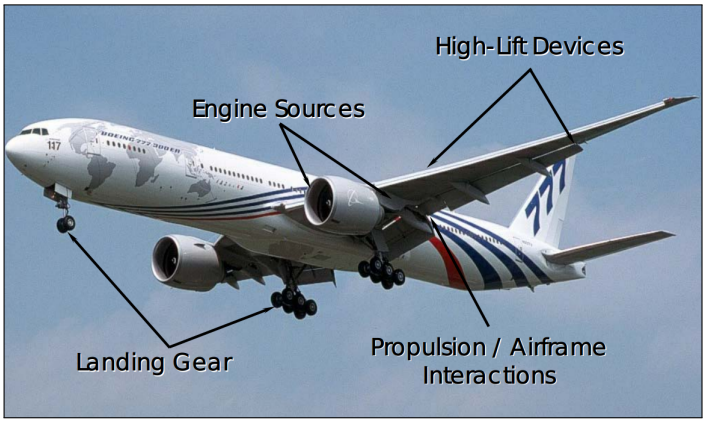

Figure 1.6: Main aircraft noise sources [16]

different generation and propagation mechanisms deserve to be investigated separately in order to have a deeper insight on each physical phenomenon involved to improve the low-noise design strategies.

1.3.1 External Noise

External noise shows a typical broadband acoustic spectrum. Such emissions come from the interaction between the turbolent airflow with the aircraft body. More in detail, high-lift

devices, such as flaps and slats, and landing gears (and with a smaller effect cavities, spoilers and turbolent boundary layers developing on the surfaces) can generate noise. Higher sound levels occur at lower altitudes where the air density is higher, however their relative relevance in the overall acoustic emission is usually low as they are overwhelmed by internal noise.

Flaps and slats are movable parts and they that extend from the trailing and leading edges of the wings respectively (see Figure 1.7). These devices are extended when the velocity is slow, such as during takeoff and landing, in order to increase lift. When these devices are extended, broadband noise at

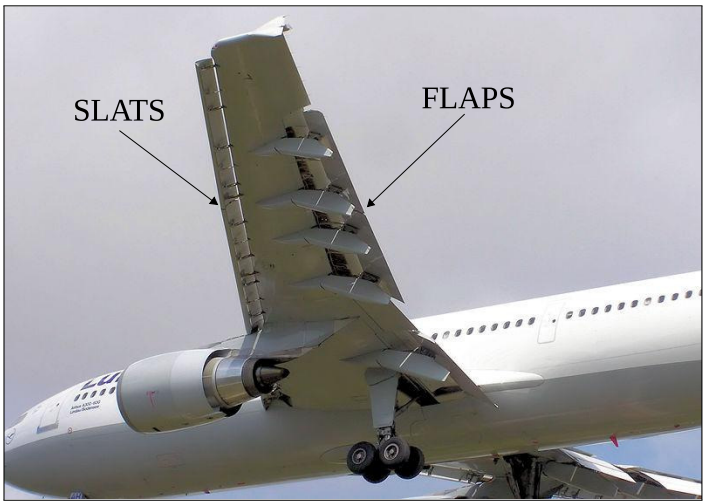

Figure 1.7: High-lift devices in aircraft wings

average and high frequency is generated because of vortex shedding and core vortex fluctuations taking place at flaps edges and in the gap between the slats and the main wing body. Effective noise reduction strategies imply low-noise design

edges for the flaps and extended seals and cover fills for the slats.

Landing gears are very complex devices, hence they generates noise over a wide range of frequencies. Turbulent and vortical flows that take place around the wheels, the gear strut and hydraulic pistons, and pin holes produce the broadband emissions. Covering these devices with fairing structures, such as toboggans, can reduce noise, but, at the same time, may cause problems in cooling the brake systems.

Figure 1.8: Toboggan fairing in landing gears [39]

In addition, also the hot jets coming from the engine exhaust impinging on the pylons that connect the engines with the aircraft are a significant source of external noise as this interaction increases the turbulence level within the jet flow itself, generating further broadband noise. For this reason, pylons are designed using low-noise strategy and acoustic

liners are installed on their surfaces to absorb part of the noise emissions.

1.3.2 Engine noise sources

Engine noise turns out to be a major source on the overall acoustic emissions. Today all the commercial aircrafts are equipped with high bypass-ratio turbofans which, as shown in Figure 1.9, emit noise from different generating mechanisms occurring both in the core and bypass jets, and in the turbomachinery components (fan, compressor, combustors and turbine).

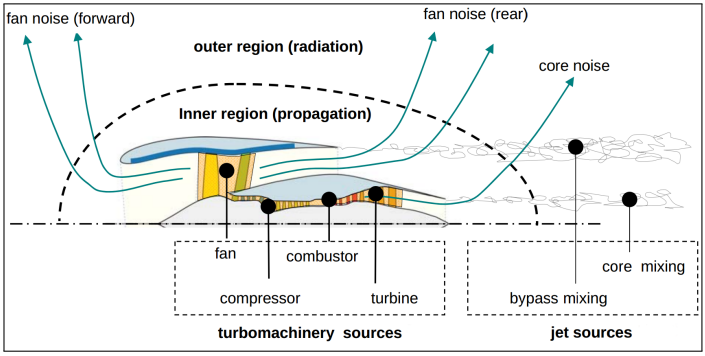

Figure 1.9: Major engine noise sources [44]

One of the major source of internal noise are the rotor-stator interactions responsible for the higher peaks in the noise spectrum at all the operating conditions. Such interactions occur in every turbomachinery part, including the low-pressure turbine. Hence, the numerical analysis of the tonal noise coming from the rotor-stator interactions in a low-pressure turbine environment is the main focus of this PhD thesis. For sake of completness, both broadband and tone noise are produced by rotor-stator interactions. The former

is characterized by a continuous spectrum covering all the frequencies. It is produced near the blade surfaces due to the

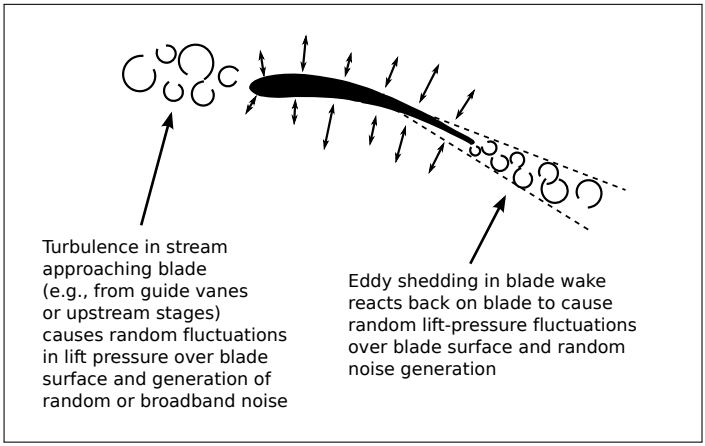

Figure 1.10: Broadband noise generation

turbulence entering the blade vane, vortex shedding at the trailing edges and sometimes by blade vibrations. All these effects cause random fluctuations of pressure (see Figure 1.10). The main sources of turbulence are the boundary layers at the enwalls, the secondary flows and the wakes produced by upstream blade rows.

Tone noise, on the other hand, can be easily identified as a succession of high-peak discrete frequency components corresponding to the so-called engine orders. Such discrete peaks arise from flow non-uniformities that interact with neighbour blade rows. Two mechanisms are involved in the noise generation: the impingement of vorticity waves due to the rotating wakes on a downstream row and the interaction of the rotating potential fields in the gap between the rows (which can travel both upstream and downstream). The noise level of each peak depends on the strength of the disturbances, which,

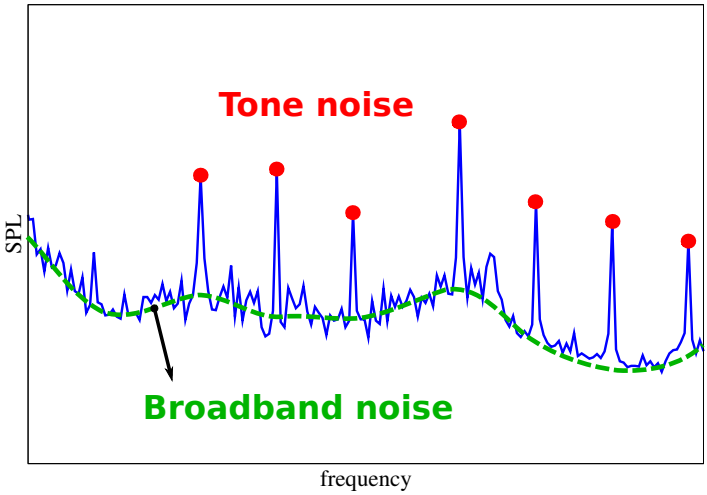

Figure 1.11: Typical LPT acoustic spectrum measured at engine exhaust

in turn, is related to the blade load. Wider axial distances between the blades reduce the emissions since mixing phenomena uniform the flow. Blade count is a key parameter as it determine the circumferential order of the acoustic spinning perturbations and hence the wave behaviour (cut-on or cut-off) when propagating within the annular duct. Finally, the wave frequencies depend on of the shaft rotational speed and rotor blade numbers and are important when radiation in atmosphere is concerned, since, as already underlined, it is highly affected by air absorption.

Jet noise

Historically, the jet has always been a very critical source of noise: in the past decades, it was by far the dominant source, today jets have become much quieter, but are still relevant at

takeoff conditions when the maximum thrust is required.

Jet noise is responsible of the typical broadband noise recognizable as the roaring low frequency sound well audible when the aircraft is flying away from the observer. Sound production is mainly located outside of the engine, in the jet plume, where high turbulence and vortexes are generated as a consequence of mixing and shear layers between the core hot jet and the bypass flow exchanging momentum with the surrounding atmosphere. For this reason it is particularly difficult to implement proper noise reduction methods.

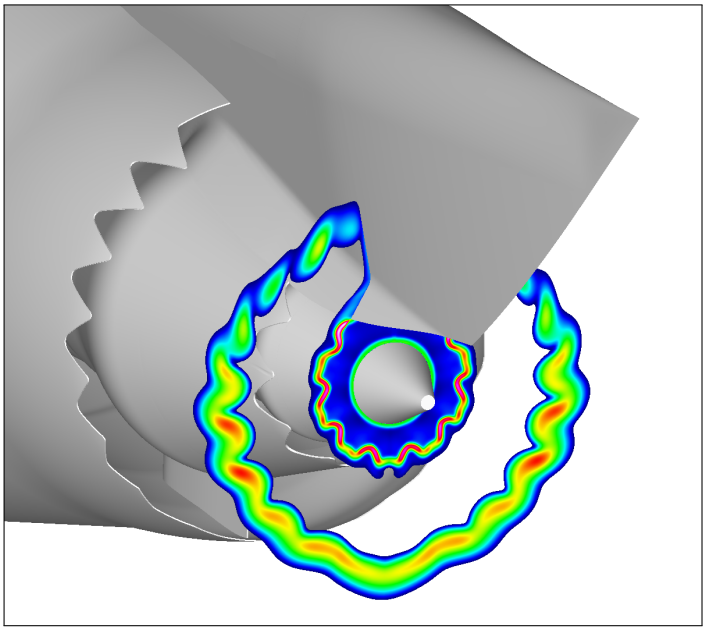

Figure 1.12: Chevron nozzles at engine exhaust [1]

Concernig the subsonic jets employed in all commercial aircrafts, noise levels varies with the eighth power of jet velocity,

that is by far the most important parameter controlling sound generation. As a consequence, the most widely used strategy to reduce jet noise consists in lowering the jet exhaust velocity as much as possible through an increase of the bypass ratio. This led to the most important noise abatement.

A further noise reduction can be achieved also by means of water injection, decreasing both the jet velocity, due to momentum transfer between the liquid and the gases, and the jet temperature due to vaporization of the injected water.

Finally, an optimization of the mixing among these three different flows may provide a significant noise reduction. To do this, chevron nozzles have been successfully employed since the late 1990s. Chevrons are sawtooth patterns placed on the trailing edge of the jet endwalls (see Figure 1.12 on the previous page) that, for separated flow nozzle, are able to decrease the jet noise without significant thrust loss.

Fan Noise

In modern high bypass-ratio turbofan engines, the fan is a major contributor to the overall noise at all the operating conditions, and the most important source at low thrust levels. Hence accurate models for fan noise predictions are necessary in order to define proper low-noise criteria.

Tone noise perturbations at the blade passing frequency and its harmonics are generated by rotor-stator interactions and propagate both upstream, through the intake channel, and downstream, in the bypass duct. Since modern fans have single stage layout, composed by one rotor and one downstream guide vane with wide blade gap, sound is mostly generated by the impingement of rotor wakes on the stator, while the interaction of pressure fields has a minor impact. In order to reduce tone noise from rotor-stator interactions at their source countless methods have been successfully developed. These strategies are aimed at reducing the number of cut-on travelling waves by means of a proper blade count selection, promoting rotor wake mixing and pressure field decay by means of wider axial

gaps and lowering noise levels by introducing leaned and swept rows.

Discrete acoustic tones can be also generated from inlet flow non-uniformities impinging on the rotor, nacelle separation or other upstream disturbances present in the intake. However the contribution of these further sources have generally a lower impact in the overall fan emissions, especially in modern engines.

When the tip Mach number exceeds the unity, shock waves occur at the leading edge of the rotor and propagate upstream producing a range of tones at multiples of the shaft frequency that are commonly referred to as "buzz-saw" noise. This noise propagates only forward and its intensity is related to the Mach number.

Soundproof panels (see Figure 1.13) are commonly placed in the intake and bypass duct. Liners have a key role in the reduction of fan noise. They consists of a perforated sheet of metal that covers cavities, typically with a honeycomb structure. Liners are designed to reduce the acoustic emissions over a range of sound frequencies through the principle of the Helmholtz resonator. Their performances depend on the depth of the cavities, hole diameters and thickness and porosity of the resistive layer.

The same principle is used in soft vanes, which are stator blades with several internal chamber covered with porous surface. Each chamber is designed to mitigate a particular tone frequency. This technology is currently used in the outlet guided vanes (OVG) within the bypass duct.

Combustion noise

As far as combustion noise is concerned, a classification between direct and indirect sound is required. The former is produced in the combustion chamber itself as a consequence of the unsteady heat release in reactive turbolent flow fields. The latter, instead, is a consequence of entropy waves generated within the combustors because of non-uniformities in

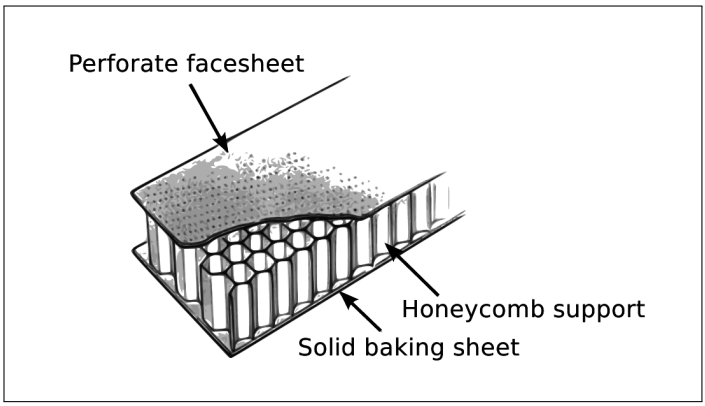

Figure 1.13: Acoustic liner for aeronautical application

temperature of the hot gases (hot spots) or imperfect mixing that propagate downstream and interact with the accelerating flow and the turbine rotating blades.

Combustion noise has typically a low frequency broadband spectrum, with higher levels in the range between 400 and 600 Hz. However some tone noise peaks can be related to indirect combustion noise. Nevertheless, its relative relevance in modern turbofan engines is quite low, often it cannot be distinguished from jet noise, being detectable only at very low power, such as idle. As a consequence it is not a priority when noise emissions are concerned.

Reduction of combustion noise can be achieved increasing the number of fuel nozzles in order to reduce temperature non-uniformities and decreasing the fuel-air ratio through a reduction of the operating pressure.

Turbomachinery noise

Turbomachinery noise is generated by compressor and turbine stages. In spite of the very different aerodynamic flow fields,

the aeroacoustic phenomena occurring in these components are very similar. The most important source of noise is the rotor-stator interaction, hence the acoustic emissions come from discrete tones being generated in all the turbomachinery stages. Tone noise can be easily identified in the engine noise spectrum knowing the rotational speed and the blade counts. Since the aeronautical gas turbines must be compact, the axial spacing between the rows is very tiny in order to reduce the engine weight and dimensions, both wakes and potential fields interactions deserve to be taken into account when evaluating discrete tones.

Usually noise emissions produced by the compressor are of minor concern, independently of the operating conditions. Indeed, since high transmission losses occur across the rows, the noise coming from the most internal stages is abated. On the other hand, the first stages can be efficiently handled exploiting cut-off design, achievable through a careful choice of blade counts and tip speeds in order to reduce the number of cut-on waves.

Turbine noise, instead, plays an important role in the overall acoustic emissions. Discrete tones propagate downstream and radiate through the shear layer between the core jet and the bypass stream. Noise reduction strategies are crucial, but hard to be implemented due to the compactness requirements and the severe environment conditions. Acoustic liners installed in the turbine nozzle, leaning and sweeping of stators (in particular the TRF: Turbine Rear Fframe) and cut-off design are the low-noise strategies commonly used during a multidisciplinar design.

1.4 Relative relevance of LPT noise

Figure 1.14 on the following page shows the relative relevance of the major aircraft noise sources at two different noise certification points. First of all, it can be observed that internal noise always turns out to be the most relevant contribution

to the overall acoustic emissions. These emissions overwhelm external noise, which, in turn, is noticeable only in approach and landing conditions when the propellers work at low power.

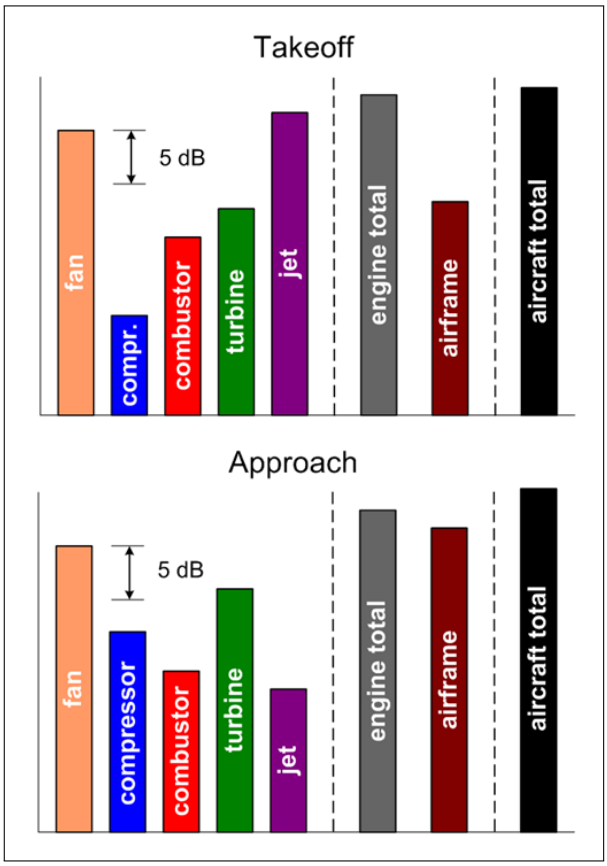

Figure 1.14: Relative relevance of aircraft noise sources at Take-off and Approach conditions [12]

Analysing the various engine sources it can be noticed

that at cutback conditions jet noise is the highest source, but also the fan has very close levels. The other components are noticeably lower. At approach conditions, instead, jet noise drops significantly as the exhaust velocities are lower. As a consequence, fan noise remains the most important source. However the low pressure turbine may significantly contribute to the overall noise as its relative relevance has constantly increased over the years. On the one hand, the acoustic levels of the most critical components (fan and jet) have been drastically reduced through the introduction of high bypass-ratio turbofan and the development of both quieter designs and more effective noise reduction technologies. On the other hand, the goal of reducing weight and dimensions of this component has been reached decreasing axial gaps blade numbers, through the introduction of profiles with higher loads. Such design solutions considerably increased the strength of rotor-stator interactions, which are the primary noise source in low-pressure turbines. Moreover, as a consequence of blade counts reduction, considering a constant rotating speed, the blade passing frequencies decrease at values where the atmospheric absorption is less efficient and so the EPNdB levels of turbine tones increase.

Further reductions in jet and fan noise are expected in the next years through the introduction of the next generation of turbofan with ultra high bypass-ratio and geared slow-speed fans. As a result the relative relevance of the low-pressure turbine noise will further increase together with the interst in accurate low pressure turbine noise prediction tools by aeronautical industry.

Chapter 2

LPT tone noise

This chapter aims to introduce some aspects of the aeronautical low-pressures turbines related to noise production. The low-pressure turbine is one of the most critical components in a modern turbofan engine: from an aerodynamic point of view, the turbine rows are composed by profiles with high loads in order to provide the required power for the fan to operate and, at the same time, to keep the engine weight as low as possible. Blades with higher loads are critical from an aeroacoustic point of view since the dominant mechanism of noise generation in low-pressure turbines are the rotor-stator interactions: the resulting noise spectrum is characterized by discrete tones corresponding to the balde passing frequencies that stands out over the broadband noise level. For this reason, an increase in blade loads usually corresponds to higher peaks. The study of the physical phenomena that govern tone noise generation and propagation is therefore crucial to develop numerical models able to predict the acoustic emissions of a turbine within the design loop.

2.1 The role of rotor-stator interactions in LPT blades

The layout of modern high bypass-ratio turbofan engines features two or three concentric shafts. Each shaft rotates with the velocity required by the driven operating component in order to ensure the highest aerodynamic efficiency. The power required from each shaft is provided by a different turbine element (see Figure 2.1). Finally, thrust is generated by the momentum variation between the inlet and exhaust of bypass and core flows.

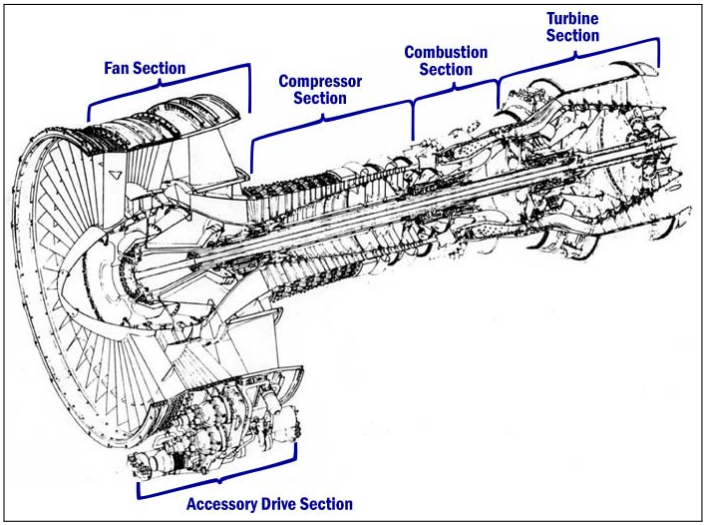

Figure 2.1: Conceptual scheme of a three shaft turbofan engine

The low-pressure turbine has to supply a large amount of power as the fan may contribute to even the 80% of the overall engine thrust. Over the years the bypass-ratios have been increased, together with the fan diameter, in order to

gain higher engine efficiencies and lower noise emissions. As a consequence, the rotational speed of the fan (and consequently of the LPT) had to be reduced to avoid excessively high tip velocities, which would entail a drastic increase in profile losses. Furthermore, the low-pressure turbine diameters are limited by geometrical constraints due to the bypass duct. For these reasons, flow velocities in LPT blade rows must be low to ensure a good aerodynamic efficiency and the power provided by a single LPT stage is low as well. As a consequence a great number of stages need to be implemented, usually between 4 and 6, resulting in increase of the low-pressure turbine weight (which may makes up even the 30% of the overall engine weight)

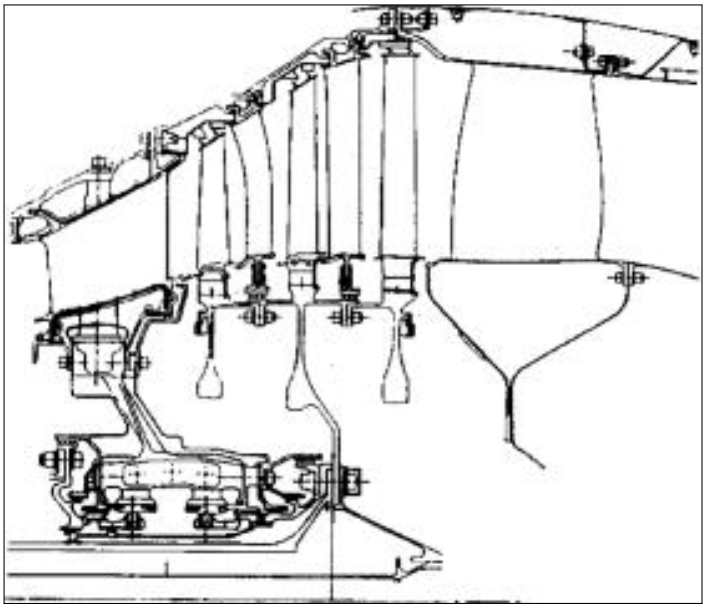

Figure 2.2: Meridional view of a LPT (BR715 GA) [21]

The main goal in designing new aeronautical engines is the reduction of fuel consumption. This can be achieved both increasing its performance or lowering its weight. Since low-pressure turbines have always been characterized by high component efficiencies, tipically well over 90%, research has been pushing toward the reduction of its weight by means of a decrease of the blade counts. To meet that target, blade loads had to be increased introducing high-lift and ultra high-lift profiles (Figure 2.3). These profiles operate under critical aero-

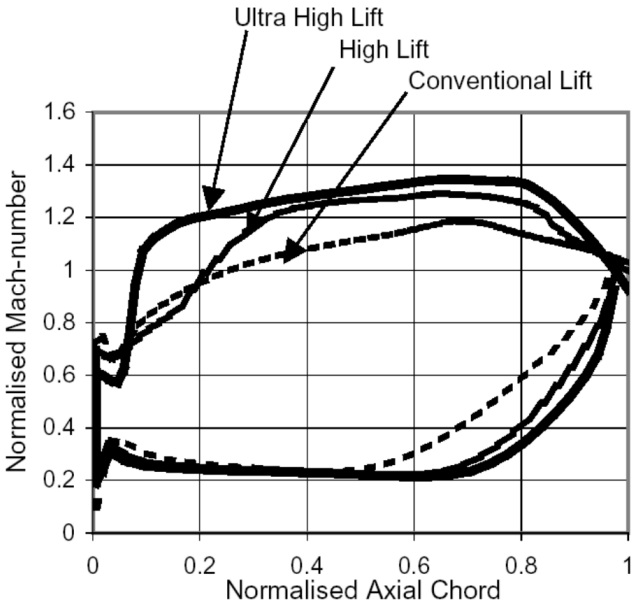

Figure 2.3: Comparison of Mach distributions on conventional, high-lift and ultra high-lift profiles [21]

dynamic conditions as the flow diffusion in the last part of the blade suction side is higher than recommended by traditional design methods. Furthermore, at the Reynolds numbers typi-

cal of low-pressure turbine environments ($05 \cdot 10^5 - 5 \cdot 10^5$), the boudary layer over a large part of the blade is laminar. A laminar boudary layer produces lower losses than a turbolent one, but it is very likely that separation bubbles (separation induced transition), with high profile loss associated, form on the suction side when isolated row configuration is concerned. However, results have shown that, when these profiles operate in the turbine, rotor-stator interaction have beneficial effects [22]: a periodic flow structure is promoted by the turbolent spots due to the wakes of the previous blade row that regularly enter the vanes and impinge on the blade suction sides. These spots promote the rapid turbolent transition of

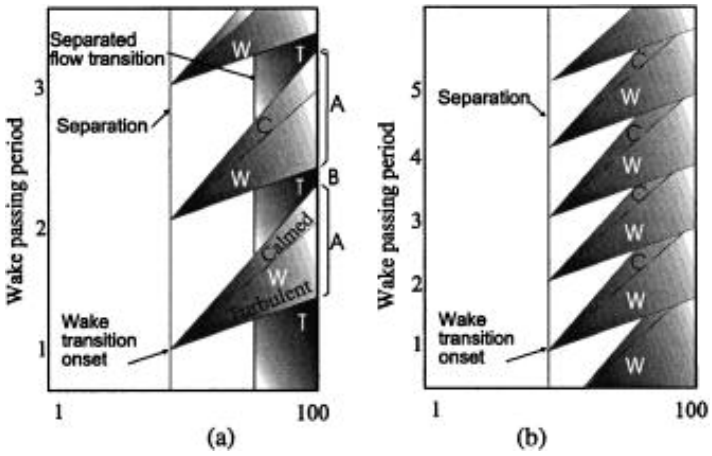

Figure 2.4: ST diagram of wake induced transition at two different reduced frequencies [22]

the boudary layer (wake-induced transition) preventing the flow separation. Moreover between two consecutive turbolent spots occurs the so-called "calmed-region", characterized by a laminar attached boundary layer with very low losses associated. If the time between two consecutive spots is suf-

ficiently short, the separation bubble does not have enough time to re-estabilish (see Figure 2.4 on the previous page). Such non-stationary working condition entails lower loss than the isolated blade configuration.

Unfortunaltely these aerodynamic improvements contribute to the increase of the low-pressure turbine acoustic emissions, as they are related to rotor-stator interactions. Moreover, the reduction of rotational speed and rotor blade counts reduced the tone frequencies to values where atmosphere absorption is less effective so that higher disturbances can reach the ground.

2.2 Tone noise phenomena in LPTs

As already introduced in chapter 1, low-pressure turbine tone noise is generated by the interaction of potential fields and wakes between adjacent rows in relative motion. Afterwards, the acoustic perturbations propagate through the machine both downstream and upstream (typically axial Mach numbers are well under sonic conditions) up to the inlet and outlet sections and finally radiate outside. Such acoustic perturbations can be splitted into spinning modes, both in the circumferential and radial directions.

All these phenomena will be described in the following sections.

2.2.1 Tone noise generation

The mechanism of tone noise generation due to rotor-stator interaction can be described considering two adjacent blade rows as shown in Figure 2.5 on the facing page. An observer in the second row reference frame perceives a pressure fluctuation at the blade passing frequency, which is different from the pressure fluctuation due to the periodic ripple of the rotor alone because of the presence of the second row.

In the reference frame of the second row, taking advan-

tage of Fourier series decomposition, the periodic pressure perturbation can be described as:

$$p = A\cos\left[m_2\theta - k_1 N_1 \left(\Omega_1 - \Omega_2\right) t + \phi\right] \tag{2.1}$$

where A is the wave amplitude, m the circumferential order, θ

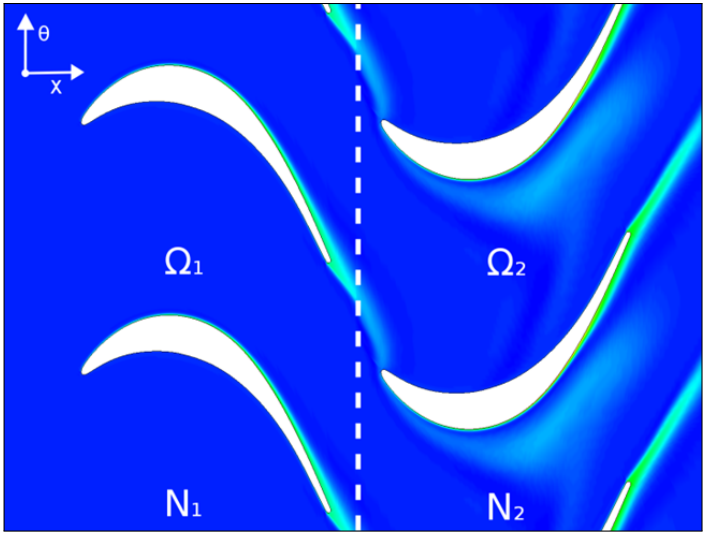

Figure 2.5: Rotor-stator interaction (entropy contours)

the angular coordinate, k_1 the harmonic order, N_1 the number of blades of the first row, $\Omega_{1,2}$ the rotational velocities of row the rows, t the time and ϕ the wave phase.

The magnitude of this pressure fluctuations depends on geometry, proximity and blade load of rows. It has the characteristic of recurring each time the rows are in an identical relative position. This means that the event happening at r, θ, t must occurs again at $r, \theta + \Delta\theta, t + \Delta t$:

$$p\left(r, \theta, t\right) = p\left(r, \theta + \Delta\theta, t + \Delta t\right) \tag{2.2}$$

Where the values $\Delta\theta$ and Δt represent the angular distance between two equivalent relative positions and the time required to reach the successive equivalent position respectively. Their values are related to the blade count of the rows and relative rotational speed as follow:

$$\begin{aligned} \Delta\theta &= \frac{2\pi}{N_2} \\ \Delta t &= \frac{2\pi}{(\Omega_1 - \Omega_2)N_2} \end{aligned} \tag{2.3}$$

Under that hypotesis, considering non-zero values of the amplitude, the following condition restricts the possible values of m_2 so that at each r, θ, t:

$$\begin{aligned} &\cos\left[m_2\theta - k_1 N_1 \left(\Omega_1 - \Omega_2\right) t + \phi\right] = \\ &\cos\left[m_2 \left(\theta + \Delta\theta\right) - k_1 N_1 \left(\Omega_1 - \Omega_2\right) \left(t + \Delta t\right) + \phi\right] \end{aligned}$$

Such a condition is satisfied if:

$$\begin{aligned} &m_2\theta - k_1 N_1 \left(\Omega_1 - \Omega_2\right) t + \phi = \\ &m_2 \left(\theta + \Delta\theta\right) - k_1 N_1 \left(\Omega_1 - \Omega_2\right) \left(t + \Delta t\right) + \phi + 2\pi k_2 \\ &m_2\Delta\theta - k_1 N_1 \left(\Omega_1 - \Omega_2\right) \Delta t + 2\pi k_2 = 0 \end{aligned}$$

Substituting equations 2.3:

$$m_2 \frac{2\pi}{N_2} - k_1 N_1 \frac{2\pi}{N_2} + 2\pi k_2 = 0$$

Hence, the allowed values of m_2 are:

$$m_2 = k_1 N_1 - k_2 N_2 \tag{2.4}$$

On the other hand, the frequency of the generated wave is given by:

$$\omega_2 = k_1 N_1 \left(\Omega_1 - \Omega_2\right) \tag{2.5}$$

Therefore, for a given harmonic order k_1, the total acoustic field generated by a rotor-stator interaction is given by a superposition of infinite rotating patterns, each one characterized

by a number of circumferential lobes given by the values of m permitted in equation 2.4 when the scattering index k_2 ranges over all the integers. Each m-lobe pattern tunrs at the rotating speed $k_1 N_1(\Omega_1 - \Omega_2)/m_2$ and propagates upstream or downstream according to its axial wave number.

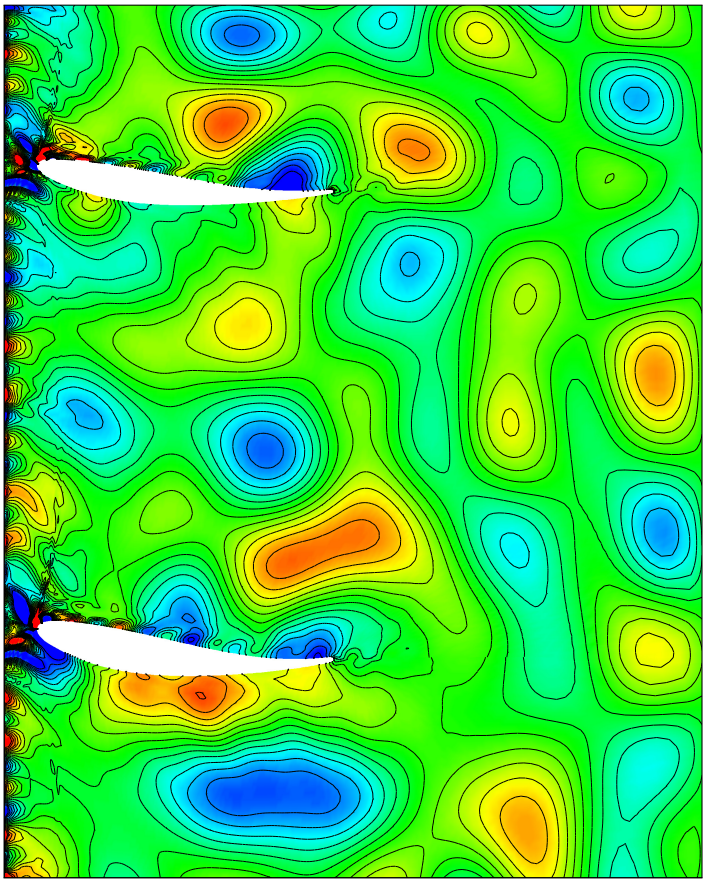

Figure 2.6: Acoustic perturbation impinging on a TRF

Similar conclusions can be drawn when considering the pressure fluctuation seen from an observer placed on the first row reference frame:

$$\begin{aligned} m_1 &= k_2 N_2 - k_1 N_1 \\ \omega_1 &= k_2 N_2 \left(\Omega_2 - \Omega_1\right) \end{aligned} \tag{2.6}$$

Figure 2.6 on the previous page shows the acoustic pressure generated by an upstream blade row impinging on a turbine rear frame. The circumferential shape of the imposed wave can easily be identified at the cascade inlet. When the fundamental wave interacts with the following row, the acoustic response is generated as a superposition of the scattered waves. It can be observed that only the modes with lower circumferential order are relevant and propagate up to the TRF exit without decaying. In the plot are also visible the effects of the convected wave coming from the upstream row: these perturbations interacts with the TRF pressure side generating further acoustic perturbations.

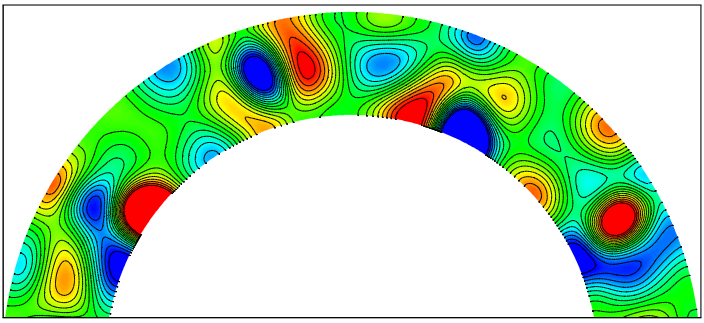

Figure 2.7: Circumferential and radia shape of the acoustic wave at TRF outlet

When considering a three-dimensional acoustic pressure field, the radial shape of the perturbation must be taken into

account as well. Figure 5.3(b) on page 74 shows the corresponding radial shape at the TRF exit. Early studies by Tyler and Sofrin [48] showed that the radial shape of these acoustic perturbations under the hypotheses of axial flow without shear and swirl can be expressed as a superposition of Bessel functions. Such assumption are too restrictive for low-pressure turbine applications, which are characterized by flow with high circumferential componentand reduced axial gaps. For this reason a more general formulation, which requires a numerical approach, must be introduced. This numerical method, described in section § 4.2.3 solves an eigenvalue problem that define radial mode shapes in a sheared and swirling flow.

2.2.2 Noise propagation

Once that the acoustic perturbations were generated, they propagate upstream and downstream from their source across the turbine rows. Different phenomena occur when the acoustic modes propagates through the inter-row annular ducts or across a blade row.

While propagating between two adjacent rows, the perturbations keep their circumferential and radial shape unchanged. In light of the physics of acoustic waves inside an annular duct, their propagation behaviour may change according to their axial wave number: if it is a real quantity the correspoding mode is called cut-on and the wave amplitude remains constant while the perturbation propagates. Otherwise, when the axial wave number is a complex quantity, the mode is cut-off and it decays during the propagation in accordance with a constant decay ratio. Obviously cut-on tones must be avoided as much as possible during the design in order to reduce the acoustic emissions of the turbine (cut-off design).

To gain insight into the waves behaviour it could be useful to prior evaluate the cut-on ranges in the inter-row regions. They can be evaluated in terms of k_2N_2/k_1N_1 ratio by means of the eigenvalue problem that governs the duct acoustics (see section § 4.2.3). To a first approximation, the cut-on/cut-off

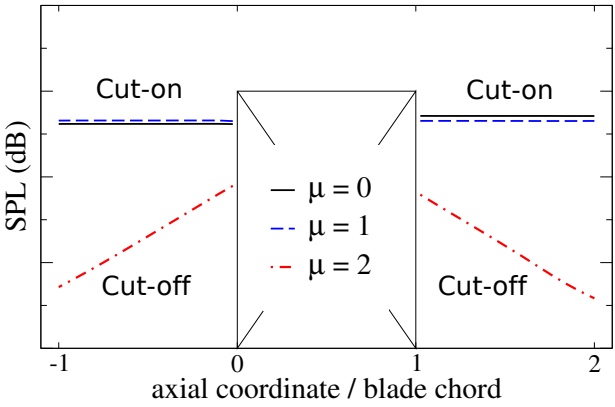

Figure 2.8: Cut-on and cut-off waves propagating downstream and upstream from a blade row

ranges can be derived from the Giles' theory [18] as well. In this theory the cut-on condition is defined by the following equation:

$$k_{\omega 2}^2 + 2k_{y2}^2 M_{y2} k_{\omega 2} - \left(1 - M_{xy2}^2\right) k_{y2}^2 \;\geq\; 0$$

where $k_\omega = \omega/a$ (a is the speed of sound), $k_y = -m/r$ and M_i are the Mach number in direction i. After some algebric manipulation the condition can be rewritten as:

$$\frac{k_2 N_2}{k_1 N_1} \;=\; 1 - \frac{M_{T2}}{M_{y2} \pm \sqrt{1 - M_x^2}} \tag{2.7}$$

where $M_{T2} = (\Omega_1 - \Omega_2) r / w_s$. Waves with the $k_2 N_2 / k_1 N_1$ ratio inside the limits defined by equation 2.7 are cut-on. These limits change along the machine as the mean flow conditions in the gaps between the rows vary as well, hence a wave can change its behaviour from cut-on to cut-off or vice versa during the propagation.

In contrast, while crossing rotor or stator blade rows, the waves interact with the lifting surfaces keeping their absolute frequency unchanged. Hence a change in reference frame (e.g. from the second to a third row) implies a change in the relative radian frequency and interblade phase angle. Considering that:

$$\begin{aligned} m_3 &= -m_2 \\ \theta_3 + \Omega_3 t &= \theta_2 + \Omega_2 t \Rightarrow \theta_3 = \theta_2 + (\Omega_2 - \Omega_3)\, t \end{aligned}$$

And taking into account the relative rorational speed and the number of blades of the two neighbour rows:

$$\begin{aligned} p &= a\cos\left[m_3\theta_3 - \omega_3 t + \phi\right] = \\ &= a\cos\left[m_3\theta_2 + \left\{m_3\left(\Omega_2 - \Omega_3\right) - \omega_3\right\} t + \phi\right] = \\ &= a\cos\left[-m_2\theta_2 + \left\{m_2\left(\Omega_3 - \Omega_2\right) - \omega_3\right\} t + \phi\right] = \\ &= a\cos\left[m_2\theta_2 - \left\{m_2\left(\Omega_3 - \Omega_2\right) - \omega_3\right\} t - \phi\right] \end{aligned}$$

The relations that allows the switch of reference frame become:

$$\omega_3 = -\omega 2 + m_2\left(\Omega_3 - \Omega_2\right) \tag{2.8}$$

$$\sigma_3 = \frac{2\pi}{N_3} m \tag{2.9}$$

Finally, when the propagating waves impinge on the following row, acoustic scattering also occurs, generating further acoustic modes with circumferential periodicity related to the impinging wave circumferential order and the number of blade of the scattering row. Scattered waves may have higher noise levels than the fundamental.

2.3 Tone noise emissions evaluation

It is common practice to evaluate and compare the acoustic emissions using two logarithmic quantities, the Sound Pressure Level (SPL) and the sound PoWer Level (PWL), which will be described in section § 2.3.1 and section § 2.3.2

2.3.1 Sound Pressure Level

Already mentioned in section § 1.1, sound pressure level is the logarithm of the ratio between the sound pressure (typically the root mean square of the acoustic pressure is used) and a reference pressure whose value is $20\mu Pa$, being the human threshold in absence of hearing impairment. It is measured in decibel (dB):

$$\text{SPL} \;=\; 20\log\left(\frac{p_{rms}}{p_{ref}}\right) \tag{2.10}$$

Where p_{rms} is given by:

$$p_{rms} \;=\; \sqrt{\frac{1}{T}\int_{t}^{t+T} p'^2 \mathrm{d}t} \tag{2.11}$$

The sound pressure level is a local value, hence it is necessary to specify where it is computed.

2.3.2 Sound Power Level

Sound power is a quantity that describes the energy transport associated to the acoustic waves. In low-pressure turbine environments, sound power is computed integrating the acoustic intensity $\vec{I}_a$ over a section of the annular duct:

$$W_{ac} \;=\; \int_{\Sigma} \vec{I}_{ac}\cdot\vec{n}\mathrm{d}\Sigma \tag{2.12}$$

The acoustic intensity can be calculated with the expression provided by Myers [32]:

$$\vec{I}_{ac} \;=\; \left(\frac{p'}{\varrho}+\vec{c}\cdot\vec{c}'\right)(\varrho\vec{c}'+\varrho'\vec{c})+\varrho\vec{c}T's' \tag{2.13}$$

Finally the sound PoWer Level (PWL) is computed as:

$$\text{PWL} \;=\; 10\log\left(\frac{W_{ac}}{W_{\text{ref}}}\right) \tag{2.14}$$

Where W_{ref} is the reference sound power in air whose value is $W_0 = 10^{-12}$W. The sound power level is measured in dB as well.

In the following analyses the PWL value will be widely used as it allows the comparison of the overall emitted noise coming from different interactions, especially when acoustic scattering occurs. Both the overall and single mode PWL will be used to to provide a comprehensive comparison with the experimental data.

Chapter 3

2D tool for tone noise prediction

Fast and robust noise prediction tools are become essential as they allow preliminary aeroacoustic analyses at the beginning of the engine design loop, when the primary design decisions have to be made. To that purpose, a 2D preliminary acoustic tool capable of a quick estimation of the acoustic emissions from a turbine has been developed at the University of Florence. The tool is composed of several modules: each module is devoted to modeling a different phenomenon of the problem (generation, propagation and transmission). This chapter describes this tool, with particular emphasis to the transmission module developed during this PhD.

3.1 Tool overview

The two-dimensional Tone Noise Tool (TNT) developed at the University of Florence is composed of several modules: the generation module, that evaluates the noise emissions due to a rotor-stator interaction between adjacent rows, the propagation module, which computes the evolution of a acoustic wave

traveling in the gap between two adjacent rows and interacting with them, and finally the transmission module, that analyses the propagation of waves across a blade row, computing, for example, the transmission and the reduction coefficient.

During the early design phase of a LPT module, the generation module is able to quickly compute the acoustic emissions at all the harmonics due to the interaction of each pair of adjacent rows. Afterwards, these acoustic waves need to be propagated up to the turbine exhaust. Wave propagation can be performed either with the transmission module, or with the propagation module. The main difference between them is that the second one can handle also the acoustic scattering, but it is more expensive in terms of computational time required. As a consequence, the transmission module is used to perform all the row transmissions except when there is the need to compute also the acoustic scattering (such as when a turbine rear frame is implemented at the turbine exhaust).

In the following sections the different modules of TNT will be described. Having been developed as one of the activities of this PhD, special emphasis will be put in the description of the transmission module.

3.2 Generation module

The generation module (named TNTgen) implements an extension from fan to low-pressure turbine applications of Hanson's coupled 2D theory [20], that, in turn, is a generalization for multiple harmonics of Smith's theory [41].

The tool computes the interaction between two adjacent blade rows evaluating the effects of the upstream blades wake impinging on the following cascade. Blade rows are modeled as 2D flat plate cascades (see Figure 3.1) and are included in a fully coupled unsteady analysis that simultaneously satisfies the flow tangency on both rows. That way, the effects of noise generation, scattering and reflection of multiple harmonics are coupled in a linear system that links the up-wash velocity

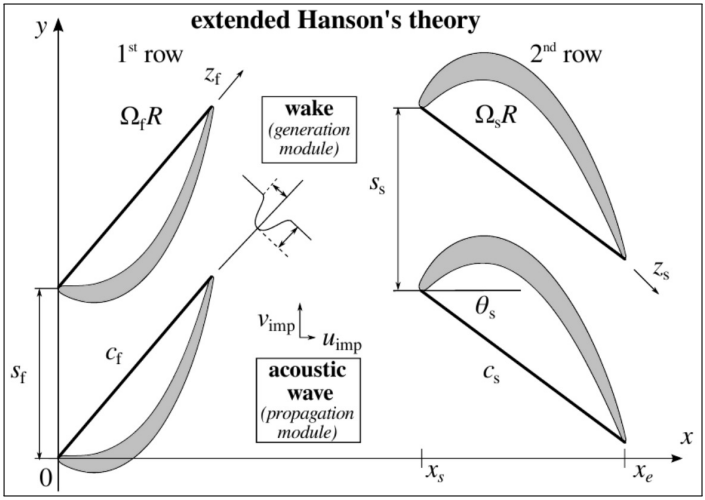

Figure 3.1: Hanson actuator disks

due to the incoming perturbation to the unsteady loading. These unsteady loadings generates outgoing acoustic waves, therefore, once they have been computed, it is simple to derive the resulting output in terms of SLP and PWL.

Swirling flow in the gap between two adjacent rows is considered in order to have a better representation of the mean flow properties and it is calculated by means of actuator disk theory. In the first version of the tool the flow field is divided into three regions: an upstream region (A) and a downstream region (C) where the flow is assumed to have axial direction, and an inter-row region (B) where swirling flow is considered. Nevertheless, the flow at the inlet and at the outlet of a typical LPT stage has high swirl components, hence a modification of Hanson's description of the mean flow has been introduced in order to consider swirling flow also in regions A and C. Since the mean flow varies across the blade

rows, the unsteady quantities vary as well. This is handled by means of reflection and transmission coefficients for all the waves taken into account in the coupled analysis and that are directly computed from the linearized continuity of mass and momentum.

Further details about TNTgen module are provided in [37] and [34].

3.3 Propagation module

The propagation module (named TNTpro) implements a minor extension of the same model described in the previous section. This extension of Hanson theory, indeed, also allows the analysis of the acoustic propagation across the following rows up to the turbine exhaust. The method evaluates the effects of the interaction between two adjacent blade rows when an acoustic wave coming from a previous generation or propagation is imposed in the inter-row gap. However, after the introduction of the transmission module (which will be described in the following section) this module has been relocated to compute the scattering at the exit of the last row.

3.4 Transmission module

This module (named TNTtrans) was developed to replace the propagation module as it is too demanding in terms of computational time. Furthermore, the transmission module has increased the reliability of the whole procedure when the waves to be transmitted are close to their cut-on/cut-off boundary.

The model proposed by Cumpsty & Marble [14], which is able to evaluate the propagation of acoustic, entropy and vorticity perturbation across 2D turbine blade rows with subsonic inlet flow has been implemented. Moreover, the tool has been extended in order to deal with rotor blades [15] as well.

The method presented Cumpsty & Marble is based on the compact row hypothesis, first introduced by Marble & Candle [28] which assumes that blade passages are sufficiently short, compared to the wavelengths, so that there is no phase difference between the flow quantities across the cascade. Also pitch-chord ratio is assumed to be low, therefore, the row is replaced by a large number of short blades, as sketched in Figure 3.2. In light of these assumptions, the two-dimensional

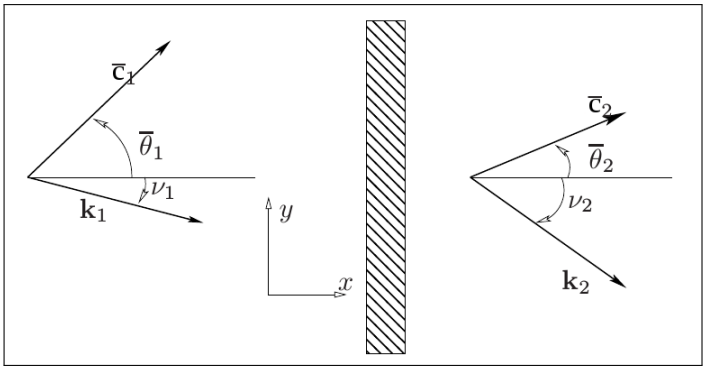

Figure 3.2: Compact row model [15]

flow fields upstream and downstream of a blade row can be described, in the undisturbed state, by means of the actuator disk theory considering the main four variables: the average velocity magnitude $\overline{c}$ and its direction $\overline{\theta}$, the average pressure $\overline{p}$, and finally the average density $\overline{\varrho}$. The small disturbances perturbing the steady flow fields may consist of two kind of convected waves, the vorticity and the entropy perturbations, and two acoustic waves traveling either upstream or downstream. Such waves are described by four primitive variables: the fluctuations of entropy s'/c_p, velocity modulus $c'/\overline{a}$, pressure $p'/\gamma\overline{p}$ and velocity angle θ'.

Although the model assumes that the blades are very short, the method can be used to propagate the waves across all the

rows up to the machine exhaust. In order to take into account the actual axial length of the turbine, appropriate axial spacings between the "compact" rows are introduced. Inside this annular area the waves are propagated in accordance with their own axial wave number.

3.4.1 Wave decomposition

To a first order approximation, the four perturbations do not interact each other, hence they can be assumed independent and can be superimposed. Each wave must satisfy the Linearized Euler Equations (LEE):

$$\frac{D}{Dt}\left(\frac{\varrho'}{\overline{\varrho}}\right) + \frac{\partial u'}{\partial x} + \frac{\partial v'}{\partial y} = 0 \tag{3.1a}$$

$$\frac{D}{Dt}\left(u'\right) = -\frac{1}{\overline{\varrho}}\frac{\partial p'}{\partial x} \tag{3.1b}$$

$$\frac{D}{Dt}\left(v'\right) = -\frac{1}{\overline{\varrho}}\frac{\partial p'}{\partial y} \tag{3.1c}$$

$$\frac{D}{Dt}\left(\frac{s'}{c_p}\right) = \frac{D}{Dt}\left(\frac{p'}{\gamma\overline{p}} - \frac{\varrho'}{\overline{\varrho}}\right) = 0 \tag{3.1d}$$

where the total derivative is defined as:

$$\frac{D}{Dt} = \frac{\partial}{\partial t} + \overline{u}\frac{\partial}{\partial x} + \overline{v}\frac{\partial}{\partial y}$$

and the mean variables $\overline{u} = \overline{c}\cos\overline{\theta}$ and $\overline{v} = \overline{c}\sin\overline{\theta}$ are the axial and circumferential components of the mean velocity. The corresponding fluctuating components, u' and v', are related to c' and θ' as follow:

$$\frac{u'}{\overline{u}} = \frac{c'}{\overline{c}} - \theta'\tan\overline{\theta}$$
$$\frac{v'}{\overline{v}} = \frac{c'}{\overline{c}} + \frac{\theta'}{\tan\overline{\theta}}$$

Expressing a generic perturbation in the form:

$$w_\phi = A_\phi e^{\left[-j\left(\omega t - \vec{k}_\phi \cdot \vec{x}\right)\right]} \tag{3.2}$$

where A_ϕ is the wave amplitude, ω the angular frequency, t the time, $\vec{x}$ the position vector in the fixed reference frame and $\vec{k}_\phi$ the wave vector of the perturbation. In this 2D model the wave vector has a circumferential and an axial component:

$$\vec{k}_\phi \cdot \vec{x} = k_{\phi,x} x + k_{\phi,y} y$$

where:

$$k_{\phi,x} = \vec{k}_\phi \cos \nu_\phi$$
$$k_{\phi,y} = \vec{k}_\phi \sin \nu_\phi$$

Once that all the waves are included in equations 3.1a-3.1d a relation between the four waves and the fluctuating primitive variables can be obtained: the following system can be written, both at the inlet and at the outlet of the row:

$$\begin{Bmatrix} s'/c_p \\ c'/\overline{a} \\ p'/\gamma\overline{p} \\ \theta' \end{Bmatrix} = \underline{\mathrm{M}} \cdot \begin{Bmatrix} w_s \\ w_\xi \\ w_d \\ w_u \end{Bmatrix} \tag{3.3}$$

where the pedices s, ξ, d and u are used to identify the entropy wave, the vorticity wave, the downstream running acoustic wave and the upstream running acoustic wave respectively. The decomposition matrix $\underline{\mathrm{M}}$ is defined as:

$$\underline{\mathrm{M}} = \begin{bmatrix} 1 & 0 & 0 & 0 \\ 0 & -j\frac{\sin\alpha_v}{K_v} & \lambda_d(K_d\cos\alpha_d) & \lambda_u(K_u\cos\alpha_u) \\ 0 & 0 & 1 & 1 \\ 0 & j\frac{\cos\alpha_v}{\overline{M}K_v} & \frac{\lambda_d}{\overline{M}}(K_d\sin\alpha_d) & \frac{\lambda_u}{\overline{M}}(K_u\sin\alpha_u) \end{bmatrix} \tag{3.4}$$

with

$$\lambda_i = 1 - K_i\overline{M}\cos\alpha_i \tag{3.5a}$$
$$K_i = k_i\overline{a}/\omega \tag{3.5b}$$
$$\alpha_i = \nu_i - \overline{\theta} \tag{3.5c}$$

Despite the kind of the imposed disturbances, the wave interaction with the blade row generally involves all the four types of wave. The outgoing waves are characterized by the same circumferential wave number of the imposed perturbation K_y. The corresponding axial components, representing the rate of change of amplitude and phase while propagating along the machine axis, can be determined by means of the dispersion equation knowing the circumferential wave number, the frequency and the Mach number.

For entropy and vorticity perturbations K_x is a real quantity and these waves are convected downstream:

$$K_{x,s} = K_{x,v} = \frac{(1 - K_y)M \sin\overline{\theta}}{M \cos\overline{\theta}} \tag{3.6}$$

Whereas for acoustic waves the dispersion equation is of second order and two values of K_x exist:

$$K_{x,i} = \frac{-\overline{M}\cos\overline{\theta}(1 - K_y)\overline{M}\sin\overline{\theta} \pm S^{\frac{1}{2}}}{1 - \overline{M}^2\cos^2\overline{\theta}} \tag{3.7}$$

where:

$$S = (1 - K_y\overline{M}\sin\overline{\theta})^2 - (1 - \overline{M}^2\cos^2\overline{\theta})K_y \tag{3.8}$$

As a consequence, for acoustic waves, it must be determined whether K_x is a real or a complex quantity and the direction of propagation. This depends on the sign of the discriminant S in equation 3.8: real values of K_x means that acoustic waves that propagate without decaying (cut-on), complex values lead to attenuated acoustic waves (cut-off). The direction of propagation can be determined by means of the sign of the net axial velocity component ($\overline{M}\cos\overline{\theta}\cos\nu_i$): pressure waves move downstream or upstream for positive or negative values of that velocity respectively.

3.4.2 Matching conditions

Once the waves have been expressed in terms of primitive variables, the acoustic behaviour of the row need to be expressed

by means of matching conditions between the upstream and downstream row locations.

Three of the four matching conditions represent the mass, enthalpy and entropy conservation laws. The last one depends on the relative Mach number at the outlet of the blade: when the flow is supersonic, a choking condition is employed, whereas when the Mach number is below the unity a condition on the outlet flow angle is imposed. Hence, for a generic stator blade row with subsonic flow at the exit, the four matching conditions are:

$$\left(\frac{s'}{c_p}\right)_1 = \left(\frac{s'}{c_p}\right)_2 \tag{3.9a}$$

$$\left(\frac{\dot{m}'}{\overline{\dot{m}}}\right)_1 = \left(\frac{\dot{m}'}{\overline{\dot{m}}}\right)_2 \tag{3.9b}$$

$$\left(\frac{{T_0}'}{\overline{T_0}}\right)_1 = \left(\frac{T_0'}{\overline{T_0}}\right)_2 \tag{3.9c}$$

$$\theta_2' = \beta\theta_1' \tag{3.9d}$$

In order to apply the above-mentioned matching conditions to the wave solution, they must be written in terms of primitive variables by means of Equation 3.3 on page 45, obtaining the following system:

$$\underline{\mathrm{E}}_1 \cdot \left\{\begin{array}{c} s'/c_p \\ c'/\overline{a} \\ p'/\gamma\overline{p} \\ \theta' \end{array}\right\}_1 = \underline{\mathrm{E}}_2 \cdot \left\{\begin{array}{c} s'/c_p \\ c'/\overline{a} \\ p'/\gamma\overline{p} \\ \theta' \end{array}\right\}_2 \tag{3.10}$$

where $\underline{\mathrm{E}}_1$ and $\underline{\mathrm{E}}_2$ are the matrices of the coefficient of the matching conditions at the inlet and outlet sections, defined as:

$$\underline{\mathrm{E}}_1 = \begin{pmatrix} 1 & 0 & 0 & 0 \\ -1 & \frac{1}{\overline{M}_1} & 1 & -\tan\overline{\theta}_1 \\ \frac{\lambda_{g,1}}{\gamma-1} & \lambda_{g,1}\left(\overline{M}_1 - \frac{\xi_1}{\overline{M}_1(\gamma-1)}\right) & \lambda_{g,1} & \frac{\xi_1}{\tan\overline{\theta}_1} \\ 0 & 0 & 0 & \beta \end{pmatrix} \tag{3.11}$$

$$\underline{\mathrm{E}}_2 = \begin{pmatrix} 1 & 0 & 0 & 0 \\ -1 & \frac{1}{\overline{M}_2} & 1 & -\tan\overline{\theta}_2 \\ \frac{\lambda_{g,2}}{\gamma-1} & \lambda_{g,1}\left(\overline{M}_2 - \frac{\xi_2}{\overline{M}_2(\gamma-1)}\right) & \lambda_{g,2} & \frac{\xi_2}{\tan\overline{\theta}_2} \\ 0 & 0 & 0 & 1 \end{pmatrix} \tag{3.12}$$

with $\lambda_g = \lambda/1 - \xi_i$.

3.4.3 Solution of the system

The equation system 3.10 on the previous page compute the response of a single cascade once incoming perturbations have been imposed. In case of subsonic flow, entropy, vorticity and downstream running acoustic waves can be imposed at the inlet, and the upstream running acoustic wave at the outlet. The imposed waves must be split in frequencies and circumferential components in order to solve the system for each single wave (k_y, ω). Given a pair of (k_y, ω), the value of the wave vector $\vec{k}$ can be calculated by using the dispersion equation. Then, the matrices $\underline{\mathrm{M}}$ and $\underline{\mathrm{E}}$ can be calculated at both sides of the blade row, obtaining an equation system with complex coefficients which, being a $4x4$ system can be easily solved by means of the matrix notation.

To simulate the real length of the LPT module, the axial gaps between the rows can be taken into account by means of a transmission matrix $\underline{\mathrm{T}}$ which computes the axial wave evolution in terms of amplitude and phase according to the wave vector:

$$[T] = \begin{bmatrix} e^{ik_{x,s}L} & 0 & 0 & 0 \\ 0 & e^{ik_{x,v}L} & 0 & 0 \\ 0 & 0 & e^{ik_{x,d}L} & 0 \\ 0 & 0 & 0 & e^{ik_{x,u}L} \end{bmatrix} \tag{3.13}$$

where L is the inter-row gap length.

The implementation of the model was carried out and validated reproducing a test case provided by Cumpsty & Marble.

This test case consists in evaluating the transmission of a single entropy wave imposed at the inlet of a turbine blade row. Flow conditions across the blade are listed in Table 3.1. Figure 3.3 on the next page shows the comparison between the results coming from our implementation and those provided by Cumpsty & Marble in terms of the pressure perturbation amplitude ratios generated by the incoming entropy wave. The very good agreement obtained both for the downstream and upstream running acoustic waves confirms the goodness of the implementation.

Flow conditions	
M_{in}	0.2
θ_{in}	0°
M_{out}	0.95
θ_{out}	70.4°

Table 3.1: Cumpsty & Marble test case: mean flow conditions at the inlet and outlet sections

3.4.4 Rotating blade model extension

More recently, an extension of this model to better analyse rotating blade rows has been proposed [15]. Since the total enthalpy is not constant in rotors, rotalpy is a more suitable quantity to express the second matching condition as it is conserved both in rotor and stator blade rows. Rotalpy is defined as:

$$I_1 = h_{t,1} - U_1 \overline{v}_1 = I_2 = h_{t,2} - U_2 \overline{v}_2 \tag{3.14}$$

where $h_{t,i}$ is the specific total enthalpy, U_i the blade velocity and $\overline{v}_i$ the circumferential component of the absolute speed (see Figure 3.4 on page 51).

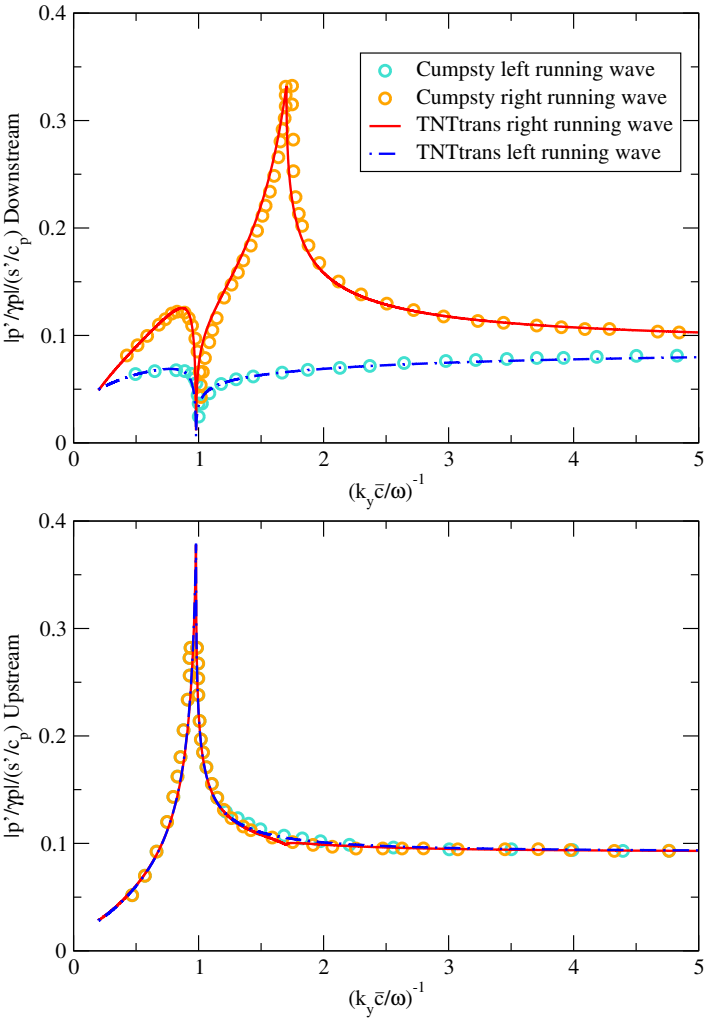

Figure 3.3: Results comparison between Cumpsy & Marble and our implementation

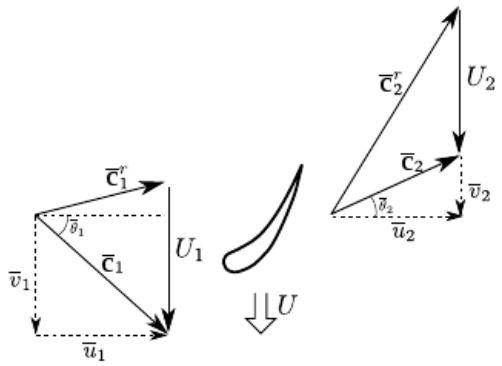

Figure 3.4: Rotating blade model: absolute and relative velocity components [15]

Under the hypothesis of small perturbations, the new matching condition can be written as follow:

$$\frac{I_1'}{\overline{I}_1} = \frac{I_2'}{\overline{I}_2} \tag{3.15}$$

with:

$$\frac{I'}{I} = \frac{h_t' - Uv'}{h_t - Uv} = \frac{\frac{h_t'}{h_t} - \frac{Uv}{h_t}\frac{v'}{v}}{1 - \frac{Uv}{h_t}} \tag{3.16}$$

and defining the parameter ξ:

$$\xi = \frac{Uv}{h_0} \tag{3.17}$$

the rotalpy, for an ideal gas, can be expressed in terms of primitive variables as follow:

$$\frac{I'}{\overline{I}} = \frac{1}{1-\xi}\left(\frac{T_0'}{\overline{T_0}} - \xi\left[\frac{1}{\overline{M}}\frac{w'}{\overline{c}} + \frac{\theta'}{\tan\overline{\theta}}\right]\right) \tag{3.18}$$

It can be observed that for stators blade rows with $U = 0$ and $\xi = 0$, the conservation of rotalpy leads to the conservation of total temperature (or equivalently enthalpy).

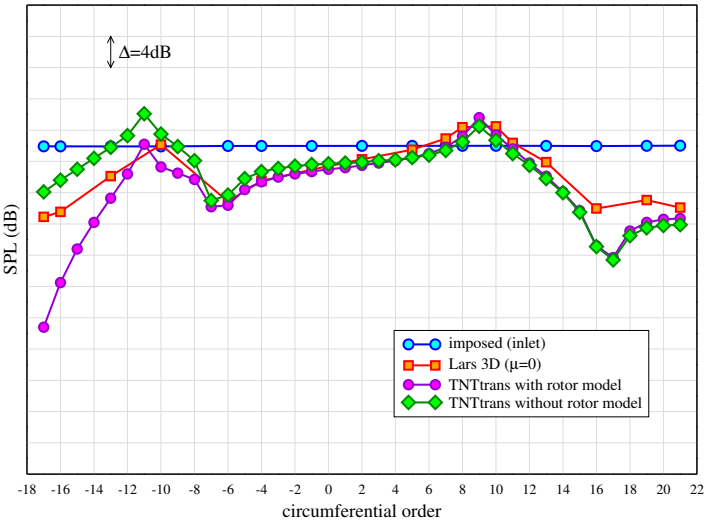

Figure 3.5: Rotor blade model: LPT test case

This extension was included in our tool and tested by predicting the noise emissions of a low pressure turbine rotor. The test was carried out imposing at the inlet of the cascade incoming acoustic waves with constant amplitude and frequency (on a reference frame relative to the blade) but with a wide range of circumferential orders. Figure 3.5 shows the amplitudes of the outgoing downstream acoustic response at the exit in terms of SPL calculated both with and without the rotating blade model. Results do not show major substantial differences between the two models, nevertheless, the comparison with 3D CAA simulations, carried out with the Lars code, shows that the rotor blade model slightly increases the capability of the tool to correctly predict the outgoing waves.

3.4.5 Comparison with 3-D results

To complete the validation of this module, (named TNTtrans) an analysis of the transmission of acoustic waves across two different low pressure turbine rows (a stator and a rotor) has been carried out. The acoustic response of each blade row has been evaluated imposing different pressure perturbations. Background dverage flow fields were representative of the typical working conditions for aeronautical low pressure turbine stages at Cutback (one of the most relevant operating points for the engine acoustic certification).

Downstream running acoustic waves with different circumferential orders and constant amplitude and frequency (on a reference frame relative to the cascade) were imposed at the inlet of each blade row to reproduce the transmission curves of each row at that frequency value. This analysis has been carried out for two different frequency values, 1000Hz and 2000Hz, in order to evaluate the prediction capabilities of the model when the frequency increases.

The transmission of an acoustic wave from the inlet to the outlet section requires the following steps:

1. Propagation from the inlet section to the blade leading edges by means of the axial wave number

2. Transmission of the acoustic wave across the blade row by means of the model described above

3. Propagation from the blade trailing edges to the outlet section by means of the axial wave number

The transmission curves obtained with this procedure in terms of both SPL and PWL are shown in Figures 3.6 and 3.7 for the stator profile and in Figures 3.8 and 3.9 for the rotor profile. The results are compared with CAA simulations performed on the same conditions with the three-dimensional time-linearized CAA solver named Lars (see section § 4.1.1).

The SPL values were easily calculated from the acoustic pressure computed by the present model by means of the usual definition provided in equation 2.10.

As far as the PWL is concerned, the axial component of the acoustic intensity is calculated with the following formula:

$$I_{a,x} = \frac{p'^2}{\overline{\varrho c}} \left(1 + \overline{M}\right)^2 \tag{3.19}$$

Afterwards, the power transport associated to the traveling acoustic waves is obtained as the product of the axial acoustic intensity I_x and the local area of the turbine duct:

$$W_{ac} = I_{a,x} A \tag{3.20}$$

Finally the PWL values can be evaluated using equation 2.14.

A very good agreement between the results of the 2D tool and the 3D simulations can be observed, in particular for the lower circumferential orders that correspond to acoustic waves that are cut-on or experience a cut-on/cut-off transition across the blade row. For these circumferential orders the differences between the TNTtrans and the CAA 3D are within a 4 dB range. On the other hand, when cut-off waves are considered, greater discrepancies can be observed. This however does not unduly affect the tool results, as cut-off waves naturally dump not being a real concern.

Finally, it can be observed that the circumferential orders where the wave behaviour changes from cut-on to cut-off are very well predicted. This is a very important result since this information is crucial for the proper selection of the machine blade counts in order to limit the number of of cut-on tones propagating up to the turbine exhaust (cut-off design). Such design parameters, indeed, are usually selected in the early design stages, where the tool is being extensively employed.

Further results of the application of the tool to the simulation of a low pressure turbine cold-flow test rig with the TNT procedure are provided in chapter 5.

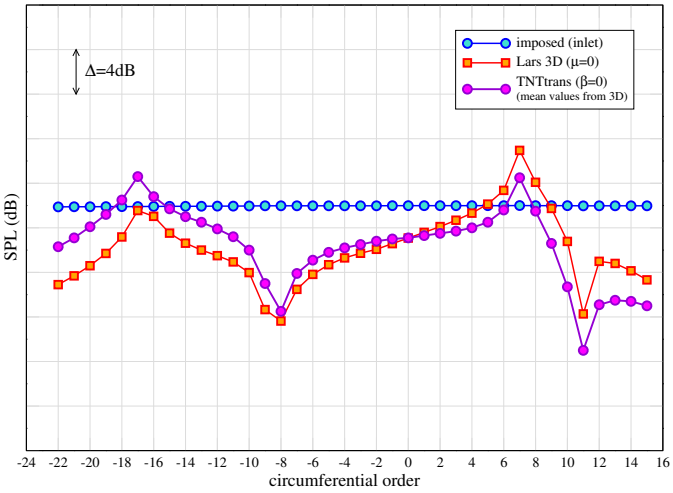

(a) SPL vs. Circumferential order

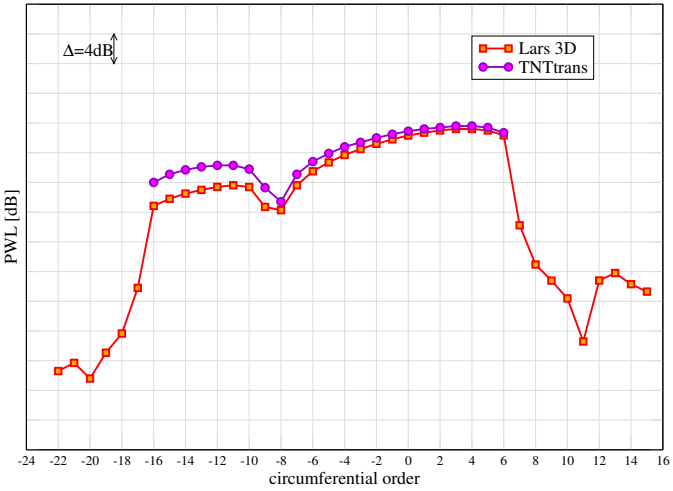

(b) PWL vs. Circumferential order

Figure 3.6: LPT test case: stator blade, f=1000Hz

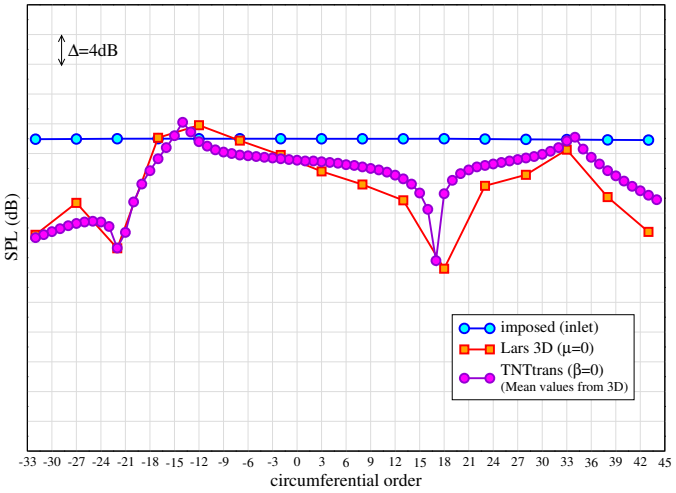

(a) SPL vs. Circumferential order

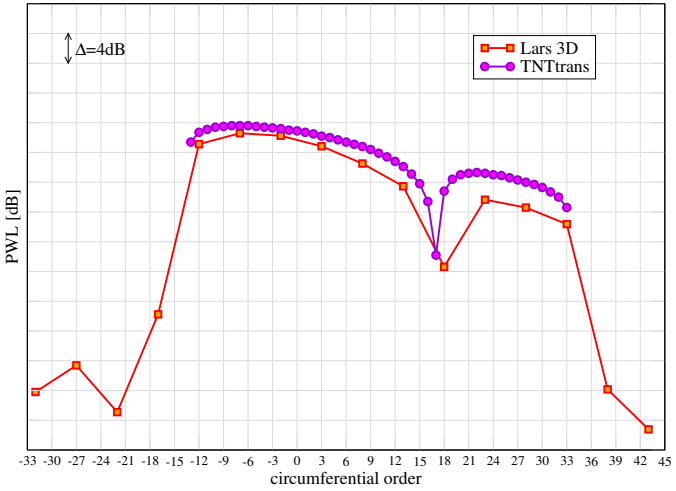

(b) PWL vs. Circumferential order

Figure 3.7: LPT test case: stator blade, f=2000Hz

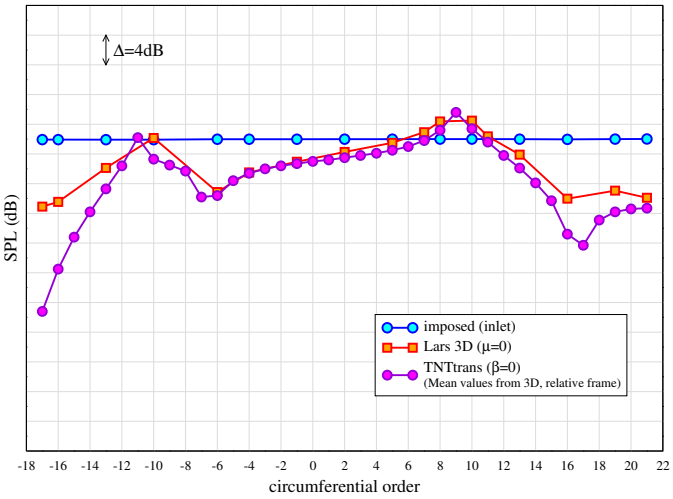

(a) SPL vs. Circumferential order

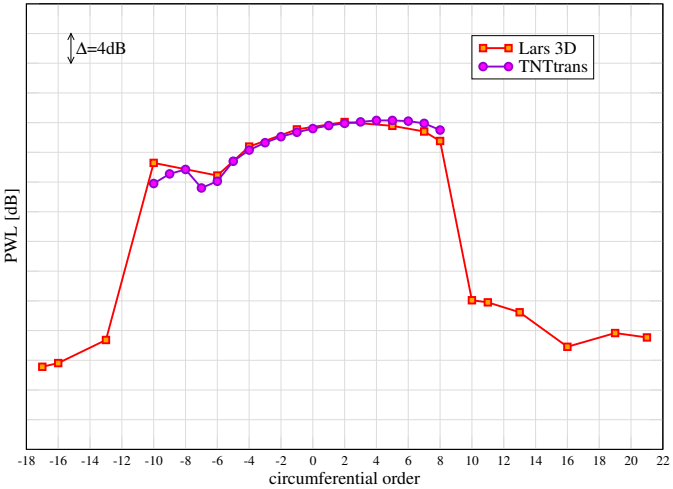

(b) PWL vs. Circumferential order

Figure 3.8: LPT test case: rotor blade, f=1000Hz

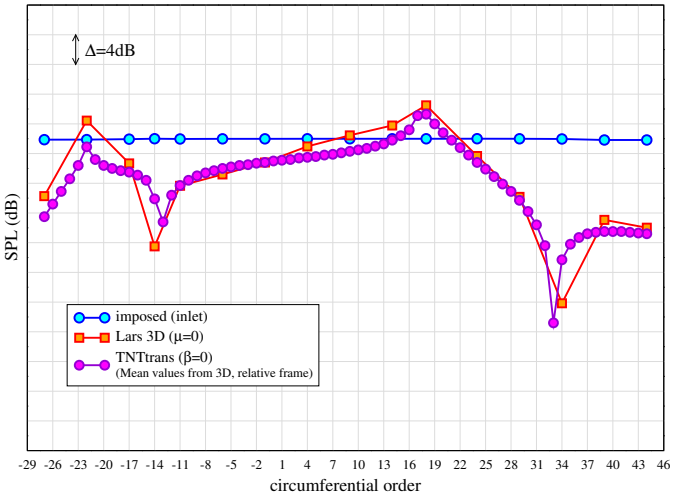

(a) SPL vs. Circumferential order

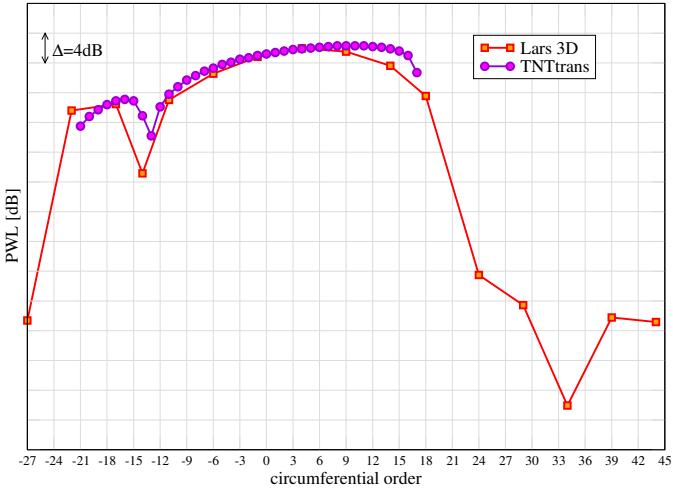

(b) PWL vs. Circumferential order

Figure 3.9: LPT test case: rotor blade, f=2000Hz

Chapter 4

3D non-linear strategy for tone noise extraction

Since the 1990s, the interest in computational aeroacoustic (CAA) methods has constantly increased thanks to the growth in computer technology. Indeed, the capability to predict the acoustic emissions coming from a component during the design phase is of great importance to develop quieter engines. Time-linearized CAA codes were the first numerical method developed as they provide reliable results with a fair computational cost. However, further increase in computer technology, together with the introduction of parallel computing, have hugely increased the computational capability. As a consequence, more detailed simulations can now be performed and the interest in more accurate methods has grown as well. For this reason, as part of the PhD activity, a procedure to extract the acoustic emissions of a low pressure turbine directly from the unsteady solution computed by a time-accurate CFD simulation has been developed. This tecnique will be described in this chapter, while a first validation can be found in chapter 5.

4.1 Aeroacoustics at DIEF

In the early 2000s at the Department of Industrial Engineering of Florence (DIEF), formerly "Sergio Stecco" Department of Energy Engineering (DEF) a new branch of research focused on computational aeroacoustic started within the research group of prof. A. Arnone.

In order to gain a deeper insight into the physical phenomena involved in aircraft engine noise generation and propagation, and thus to improve the low-noise design criteria, the research efforts are focused mainly on the analysis of turbomachinery tone noise, with the aim at developing reliable prediction tools. These tools range from a two-dimensional method named TNT for a fast evaluation of tone noise emission (already described in chapter 3) to a time-linearized three-dimensional CAA procedure that will be described in section § 4.1.1 of this chapter. Thanks to these methods a depper insight into tone noise generation and propagation phenomena in turbomachinery environments can be gained.

In this context, the first aim of this PhD thesis has been the identification of possible improvements of the existing softwares and, if needed, the development new ones. After a detailed literature review, it has been decided to work on the implementation of the two-dimensional tool form acoustic waves transmission (see section § 3.4) and of a post-processing tecnique able to extract the tone noise emissions from a non-linear unsteady CFD simulation that will be described in section § 4.2.

4.1.1 Time-linearized method for tone noise prediction

The time-linearized aeroacoustic procedure for the evaluation of tone noise generation and propagation in turbomachinery environments has been developed at the Department of Industrial Engineering of Florence (DIEF).

Such a method consists of a multistep procedure (see

Figure 4.1) based on the 3D time-linearized aeroacoustic and aeroelastic solver Lars [38]. Lars code is able to deal with incoming perturbations due to unsteady interactions with adjacent rows. Non-reflecting boundary conditions based on radial mode decomposition are used at domain boundaries in order to avoid spurious reflections.

The procedure works as follow: first of all, the rotor-stator interactions that generate the tone noise peaks must be identified in order to find where noise is generated and whether acoustic scattering occurs during the propagation. Then, a steady CFD simulation of the whole machine is required in order to obtain the mean flow field, which represents the frozen background for the following linearized computations and provides the perturbations due to wakes and potential fields in the axial gaps between the generating rows. Such perturbations are extracted by means of a wave splitting method [53] based on radial modes decomposition and imposed as incoming perturbations at the receiving row. These pre-processing steps allow the evaluation of the acoustic generation by using a time-linearized CAA computation. Finally, the relevant tones are propagated across the following rows up to the turbine exhaust by means of a sequence of time-linearized CAA simulations. In each propagation the imposed perturbation is obtained from the previous CAA computation.

Throughout this PhD thesis the results provided by this method have been used to validate the afore-mentioned 2D and 3D tools.

Further details about this procedure can be found in [36].

4.2 Non-linear CAA approach

Thanks to the continuous growth in computer technology, time-accurate CFD simulation has recently become an interesting opportunity in the field of turbomachinery design. The capability to perform unsteady computations in a relatively short time breaks new grounds and so also aeroacoustics anal-

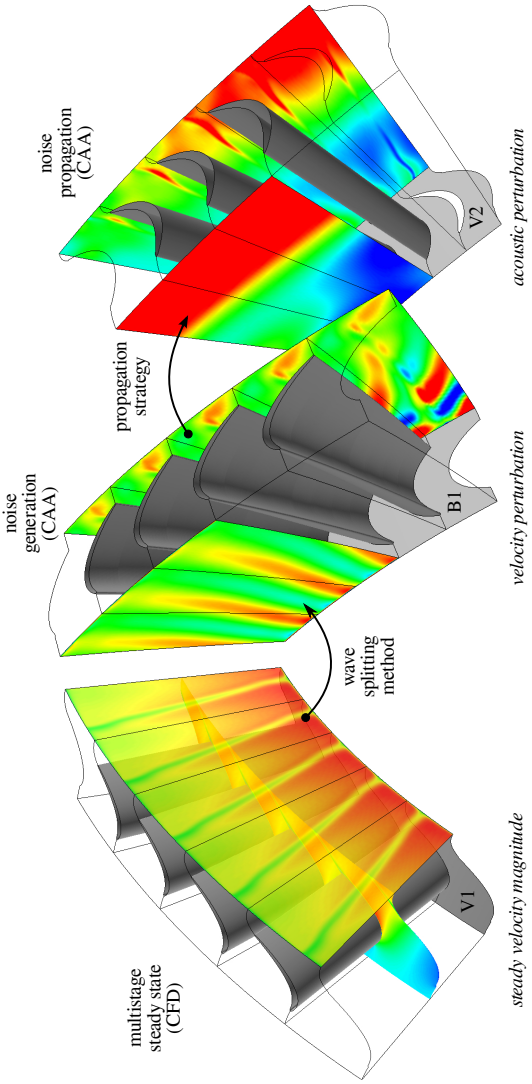

Figure 4.1: Linearized noise prediction method

ysis performed by a non-linear unsteady method become a viable alternative. Time-depending CFD solutions already contain all the informations about the pressure fluctuations generated by rotor/stator interactions and which can be decomposed in acoustic traveling waves, provided that the time and space discretizations are sufficiently accurate. For these reasons, the idea of extracting tone noise information directly from the unsteady CFD solutions by means of proper post-processing procedure has become more and more attractive by the aeronautical industry and already different procedures can be found in the literature [53, 50, 54]. Such techniques intrinsically solve all the interaction phenomena, taking into account multiple reflections and non-linear effects. On a contrary, linearized approaches may lead to wrong predictions if some of these aspects (e.g. a wide set of multiple reflections) are not included [2].

The CAA strategy developed in this PhD (sketched in Figure 4.2 on the following page) is able to evaluate the tone noise generation in turbomachinery environments. After the identification of the potentially most relevant rotor/stator interactions, each pair of generating rows must be simulated separately by means of a time-accurate CFD computation. In the present work, CFD computations have been performed with the Traf code, which will be described in section § 4.2.1. Before all, it is important to select a suitable number of time-steps per rotor revolution. The time-step size must be chosen such that the time scales of interests are solved accurately. The minimum number of time-steps required to analyse a single blade passing frequency depends on the numerical scheme implemented in the CFD code [19]. Furthermore the DFT procedure requires the number of time-steps which covers a perturbation period to be a multiple of the blade counts.

Once that the unsteady interaction flow has been computed, acoustic pressure fields must be extracted for fixed frequencies. This is performed by means of Discrete Fourier Transform (DFT) in time of the time-depending CFD solu-

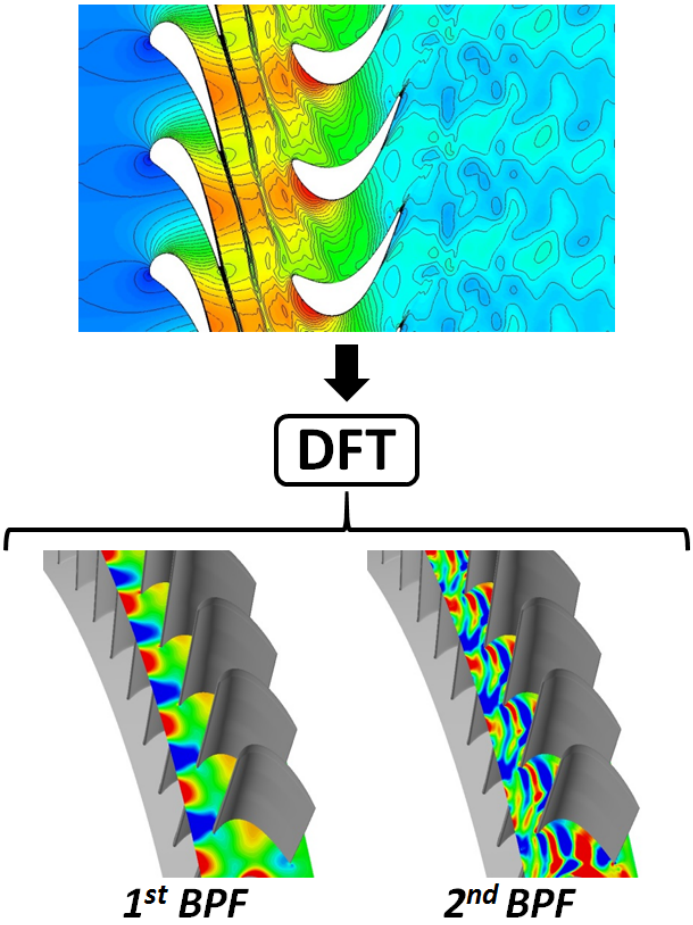

Figure 4.2: Non-linear noise prediction procedure

tion, obtaining the perturbed flow quantities in the frequency domain at the various blade passing frequencies (BPF). The DFT can be easily implemented in the CFD code in order to be executed during the last time-period, once that the solution is periodic. Afterwards, noise levels in terms of SPL and PWL can be calculated by means of a post-processing method based on the splitting of the acoustic perturbations into circumferential and radial modes (more details are provided in section § 4.2.3).

Further acoustic propagations across the following rows cannot be performed so far with this procedure. Although the whole turbine might be simulated in order to gain insight into both generation and propagation phenomena, such an approach is currently not feasible for two main reasons. First of all, the complexity of this kind of simulation would affect its reliability, especially as the perturbations of interest are small compared to other quantities. Secondly, a full-annulus computation would demand an outrageous time, even with a high parallelized CFD code running on a dedicated cluster. Taking advantage of the phase-lagged boundary conditions to run single passage computations (drastically reducing the computational time required) would not be worthwhile. Phase-lagged boundary conditions only takes into account the mutual interactions of each block with the adjacent ones, hence perturbations are not propagated further. For these reasons, acoustic propagation is handled by means of the time-linearized procedure described in section § 4.1.1.

4.2.1 Traf code description

Traf code has been employed to perform the aerodynamic simulations. It is a three-dimensional CFD code which solves the unsteady Reynolds-Averaged Navier-Stokes (URANS) equations in conservative form. It has been developed at the Department of Industrial Engineering of Florence for the aerodynamic analysis of turbomachinery flows. Detailed descriptions of the numerical methods implemented in the code are provided

in [3, 4, 5, 8, 9].

The compressible URANS equations, mapped in a curvilinear coordinate system, are solved in the relative frame with a multiblock approach. Spatial discretization is based on a cell-centred finite volume scheme. The governing equations system is advanced in time by means of an explicit four stage Runge-Kutta scheme [27].

Three techniques to reduce the computational cost and speed-up the convergence to steady state solutions are implemented in the code: local time-stepping, residual smoothing and multigrid.

Time-accurate calculations are performed through a dual-time-stepping method [6, 26] where multigrid scheme is used rewriting the equations in order to include the partial derivative with respect to time as production terms. Single passage unsteady simulation are available taking advantage of the phase-lagged boundary conditions to handle periodicity: in particular the chorocronic periodicity conditions of Gerolymos et al. [17] are used.

Artificial dissipation terms, consisting of a blending of second and fourth order difference terms, are introduced to increase the stability of the scheme regarding numerical instabilities, such as odd/even node uncoupling due to the low physical dissipation level that characterize real flows; both scalar [25] and matrix [47] artificial dissipation models are implemented together with the eigenvalue scaling [45, 29].

To model the effects of turbulence, some of the most common models are available. Turbulence models range from the algebraic formulation (Bladwin-Lomax [11], two-layer mixing length [7]), to one and tow equation models (Spalart-Allmaras [42], Spalart-Shur [43], $k-\omega$ in both high- and low-Reynolds formulation [51, 52] and $k-\omega$ SST [30]).

Traf code has a hybrid parallelism obtained from the coupling of MPI and OpenMP parallelism.

4.2.2 Discrete Fourier Transform

This section aims at introducing, for sake of completeness, the Discrete Fourier Transform (DFT). Only a general description is provided, further details can be found in dedicated literature [13, 40].

The discrete Fourier transform is the equivalent of the continuous Fourier transform for signals known only at equally spaced positions. Therefore it allows the conversion of a generic function from the physical domain (usually the time) to the frequency domain. For this reason the DFT is particularly useful for the spectral analysis of time-depending signals, such as acoustic perturbations.

Given a set of samples $\{X_n\}$, with $n = 0, 1, \cdots (N-1)$, its discrete Fourier transform is defined as another set of coefficients $\{F_k\}$ of a linear combination of complex sinusoidal components:

$$F_k = \sum_{n=0}^{N-1} X_n \mathrm{e}^{-j2\pi nk/N} \qquad k \in \mathbb{Z} \tag{4.1}$$

where $j^2 = -1$ and $F_k \in \mathbb{C}$ is the k-*th* coefficient of the DFT: a complex number containing informations about both the amplitude A_k and phase ϕ_k of the k-*th* sinusoidal component of the function X_n:

$$A_k = \frac{|F_k|}{N} = \frac{\sqrt{\mathrm{Re}(F_k)^2 + \mathrm{Im}(F_k)^2}}{N} \tag{4.2a}$$

$$\phi_k = \arctan\left(\frac{\mathrm{Im}(F_k)}{\mathrm{Re}(F_k)}\right) \tag{4.2b}$$

The frequencies of the sinusoidal components are the integer multiple of a fundamental frequency (which corresponds to the sampling frequency).

4.2.3 Radial mode decomposition in sheared and swirling flows

In chapter 2 the basis of tone noise mechanics have been described. In particular, it has been underlined that the overall emissions at a given frequency are the result of the sum of acoustic modes, both in circumferential and radial direction. Hence, the global acoustic solution provided by each harmonic of the DFT need to be further decomposed with a suitable procedure in order to identify the most critical modes. This method was first developed to be used by the non-reflecting conditions of the time-linearized approach, but it can be used also to compute the modal basis from the non-linear average solution in the frequency domain.

In presence of sheared and swirling flows [31, 49], such as in low-pressure turbine environments, the mode decomposition requires the solution of the eigenvalue problem governing the physics of waves in an annular duct. Under these hypotheses, this problem cannot be solved analytically and requires a numerical approach. Considering the Euler equations in cylindrical coordinates:

$$\frac{\partial \underline{U}'}{\partial t} + \frac{1}{r}\frac{\partial \left(r\underline{F}'_x\right)}{\partial x} + \frac{1}{r}\frac{\partial \underline{F}'_\theta}{\partial \theta} + \frac{1}{r}\frac{\partial \left(r\underline{F}'_r\right)}{\partial r} \;=\; \frac{1}{r}\underline{Q}' \qquad (4.3)$$

which can be split into the finite mean term and the infinitesimal perturbation assuming that the mean radial velocity is negligible, and that other mean flow quantities only depends on the local radius, the perturbed equations results:

$$j\omega\underline{\overline{U}}' + \frac{1}{r}\frac{\partial \left(r\underline{A}\,\underline{\overline{U}}'\right)}{\partial r} + \frac{1}{r}\underline{B}\frac{\partial \underline{\overline{U}}'}{\partial \theta} + \underline{C}\frac{\partial \underline{\overline{U}}'}{\partial x} - \underline{D}\,\underline{\overline{U}}' \;=\; \underline{0} \quad (4.4)$$

Searching for solutions in the following form:

$$\begin{aligned} \underline{\overline{U}}_\delta \;&=\; \underline{\mathscr{U}}\, e^{\,j\,(k_x\,x+\ell\,\theta)} \qquad \underline{\mathscr{U}} \;=\; \underline{\mathscr{U}}\,(r) \\ k_x \;&=\; k_x\,(r) \qquad \ell \;=\; \frac{2\pi q+\sigma}{G} \end{aligned} \qquad (4.5)$$

two categories of solutions can be obtained:

- solutions of purely convected modes propagating within the mean flow with a well defined axial wave number ($k_x = k_x(r)$).
- solutions with constant axial wave numbers which must satisfy the discretized equation:

$$(\underline{P} - j\, k_x\, \underline{C}_b)\, \underline{\mathscr{U}}^R \;=\; \underline{0} \tag{4.6}$$

These solutions represents the convected and acoustic modes that must be properly classified.

Further details about this procedure can be found in [38].

Chapter 5

Cold-flow acoustic test rig analysis

A cold-flow test rig aimed at investigating tone noise generation and propagation in low pressure turbines has been characterized. This test rig allows to gain a deeper understanding of the aeroacoustic phenomena since it provides a detailed set of experimental data directly related to the generating turbine not being affected by the presence of whole propulsion system. For this reason, the acquired measurements are particularly useful for the validation of noise prediction tools. This chapter provides a description of the test rig and its acoustic characterization performed with the noise prediction tools described in chapter 3 and 4.

5.1 Acoustic test rig

The cold-flow is an acoustic test rig which reproduces the last stages of an aeronautical low pressure turbine. It has been designed specifically to study noise generation and propagation taking advantage of engine-to-rig similitude criteria: blade geometries, loadings and flow deflections have been selected

so as to reproduce the state-of-the-art of high-lift profiles

Figure 5.1: Cold-flow rig

currently installed in low pressure turbines. Blade counts guarantee aeroacoustic similitude in terms of reduced frequency as well. Finally, as for the last low pressure turbine stages, endwalls have constant radii (see Figure 5.2 on the next page). Their dimensions have been selected to operate both at the typical conditions for noise certification (approach, cutback, sideline) and at the aerodynamic design point. The turbine discharges at atmospheric pressure, while the inlet pressurization is provided by a compressor.

The rig is characterized by a modular layout allowing the easy replacement of the rows, the variation of axial spacings and the addition of rows. Both single and two stage setup are allowed, as well as inlet or outlet guided vanes may be implemented. Thank to this feature, different turbine configurations can be analysed in order to identify the major design parame-

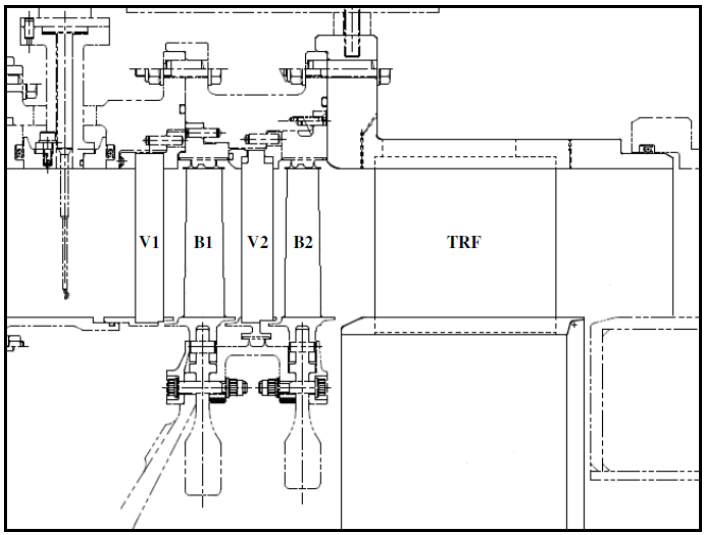

Figure 5.2: Cold-flow rig: meridian view

ters affecting tone noise generation and propagation and to study the effectiveness of low-noise strategies (in particular acoustic liners and 3D blade design).

The rig configurations analysed in this thesis consist of two turbine stages followed by a leaned TRF (Figure 5.1 on the following page) for the analysis described in section § 5.3 on page 84 and with a radial TRF for the analysis described in section § 5.4 on page 90. Blade counts, listed in Table 5.1 on page 75, have been determined in order to generate both acoustic modes with lower circumferential order, which remain cut-on at all the turbine operating points, and with circumferential orders near the cut-on/cut-off boundary, which change their behaviour depending on the working condition.

The rotor-stator interactions generating the relevant acous-

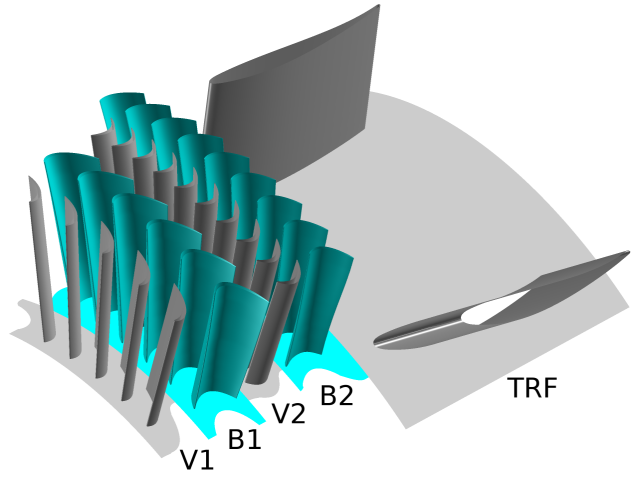

(a) leaned TRF

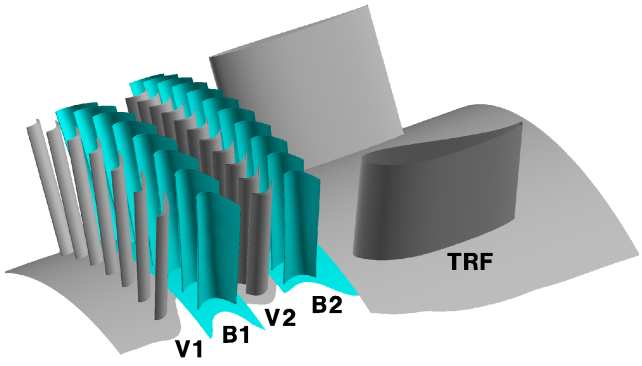

(b) radial TRF

Figure 5.3: Cold-flow rig: geometry layouts

tic tones at the $1 \times$ BPF and $2 \times$ BPF are listed in Table 5.2. Those analysed in the following sections are highlighted in bold. The circumferential order corresponding to each interaction can be easily calculated from the blade counts. However, each interaction shows a large number of cut on waves at the turbine exhaust as a consequence of the acoustic scattering occurring when pressure perturbations propagates through the TRF. This large number of scattered cut-on waves is determined by the low blade count characterizing such rows with structural function.

1^{st} stage		2^{nd} stage		
1^{st} stator	1^{st} rotor	2^{nd}stator	2^{nd} rotor	rear frame
V1	B1	V2	B2	TRF
64	68	112	88	9

Table 5.1: Cold-flow rig: blade counts of the rows

frequency	interaction	behaviour
+1B1	**+1V1-1B1**	**cut-on**
+2B1	+2V1-2B1	cut-on
+1B2	+1V2-1B2	cut-off/cut-on
+1B2	**+1B2-TRF**	**cut-on**
+2B2	+2V2-2B2	cut-off/cut-on
+2B2	+2B2-TRF	cut-on

Table 5.2: Cold-flow rig: rotor-stator interactions responsible for the tone noise emissions at turbine exhaust (analysed interactions are highlighted in bold)

Shown in Figure 5.4 on the following page are the operating points analysed during the last experimental campaign. Those working conditions have been selected on the performance

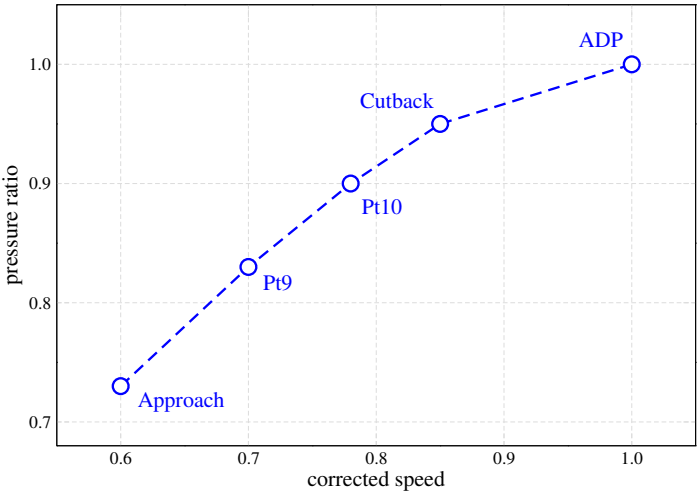

Figure 5.4: Cold-flow rig: performance curve

curve in order to reproduce the typical working conditions for the noise certification points (approach and cutback) together with the Aero Design Point (ADP) and two other intermediate points (pt9 and pt10).

The acoustic measurements acquired during previous experimental campaigns carried out at the cold-flow test rig have already proven to be very useful for the validation of CAA tools for tone noise prediction [34, 35]. Indeed, such test rig allows to gather a detailed insight of the aeroacoustic phenomena occurring in a low pressure turbine environments since noise emissions can be recorded directly inside the turbine nozzle. Moreover, the acoustic emissions of such a test rig are not affected by the presence of other engine noise source (i.e. fan, compressor, jet and core). In this thesis the measurements acquired during the last cold-flow experimental campaign carried out at the Avio facility have been used to validate the numerical tools developed during the PhD.

5.1.1 Noise measurements

Acoustic instrumentation consists of a rotating duct section installed within the turbine exit that allows a detailed mapping of the 3D acoustic field by means of two radial rakes of piezoresistive Kulite pressure sensors with uniform spacing in the radial direction (see Figure 5.5).

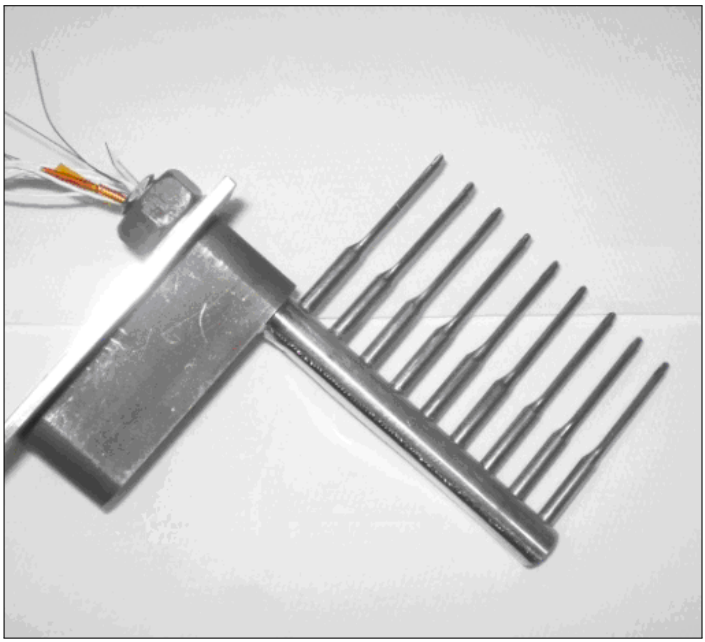

Figure 5.5: Cold-flow rig: radial rake

At each operating condition, the number of azimuthal position of the rakes are selected in order to to collect a sufficient number of acoustic data along the circumferential direction, so as to detect all the relevant cut-on modes. High speed acquisition hardware allows the simultaneous acquisition of all the unsteady pressure signals. Additionally, one pulse per

revolution is recorded for synchronous re-sampling purposes, since it increases the signal-to-noise ratio and improves the global accuracy, avoiding detrimental effects due to rotor speed variations during the measurements. Also axial arrays of flush-mounted capacitive microphones are available to confirm the Kulite measurements at low and mid frequency values.

Since mean flow field measurements are required both to identify the turbine operating conditions and to perform Radial Modal Analysis (RMA) that compute the acoustic modal basis, aerodynamic instrumentation has been installed as well.

Further details about the experimental setup are provided in [46].

5.2 Mean aerodynamic results

Steady CFD simulations are required to perform CAA simulations: the time-linearized CAA code needs a frozen background both to extract the perturbations to be imposed (by means of the wavesplitting procedure) and to compute the perturbed solution. The non-linear procedure uses the steady solution as initialization for the time-accurate rotor/stator simulations. Also the TNT requires the mean flow values provided by the steady state CFD.

The aerodynamic simulations have been performed with the Traf code at the operating conditions reported in Figure 5.4 on page 76. Single-block elliptic H-type periodic grids have been used. Figure 5.6 on the next page shows a blade-to-blade view of the computational meshes. Their dimensions, listed in Table 5.3 on page 80, have been selected in order to meet both the aerodynamic and aeroacoustic requirements. Wall re-clustering for boundary layer were chosen so that the $y+$ values of the mesh cells closest to the wall were below unity. The same grids have been used also for the aeroacoustic simulations that will be described in the following sections.

Boundary conditions for the aerodynamic simulations, con-

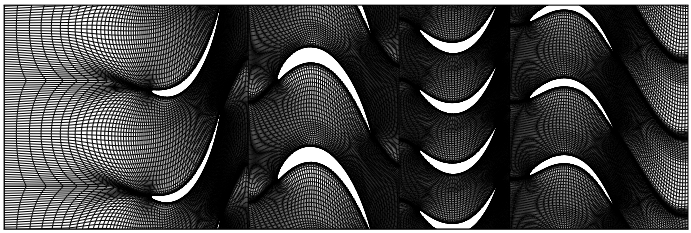

(a) 1^{st} and 2^{nd} stage

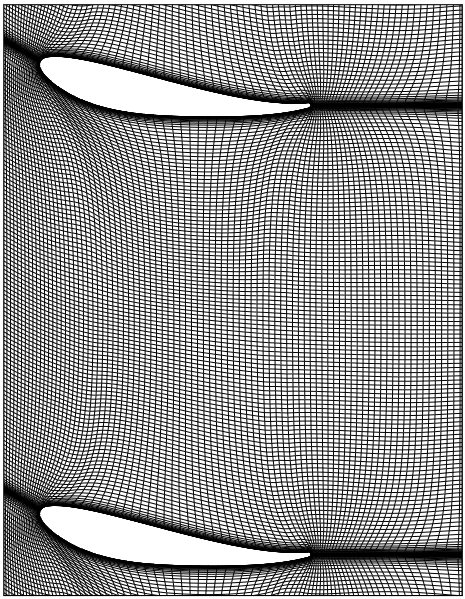

(b) TRF

Figure 5.6: Cold-flow rig: blade-to-blade view of computational mesh (different scale factors, grid dimensions were reduced for a clearer visualization)

sists of the spanwise distribution of the total pressure and flow angle at the inlet section, and static pressure at the exhaust. They have been selected in order to reproduce the same working conditions measured during the experimental campaigns.

Finally, the $k-\omega$ turbolence model in the high-Reynolds formulation has been employed as previous studies indicated that it provides a better representation of the wakes diffusion, which is essential to correctly predict the rotor-stator interactions responsible for tone noise generation [34].

Row	Grid dimensions
V1	264× 88×100
B1	248× 88×100
V2	248× 88×100
B2	300× 88×100
TRF	256×140×100

Table 5.3: Cold-flow rig: cell numbers of the computational meshes in the x, y, z directions

Figure 5.7 shows the pressure contours at blade mid-span (cutback conditions). Pressure distribution comparisons between the numerical simulations and the measurements at three different spans are shown in Figures 5.8 and 5.9. Such comparisons, available at approach and cutback conditions for the first stator vane, shows a very good agreement between code results and the experimental data. Other flow quantities such as the mass flow, are in good agreement with the measurements, hence these steady simulations are a proper starting point for the following aeroacoustic simulations.

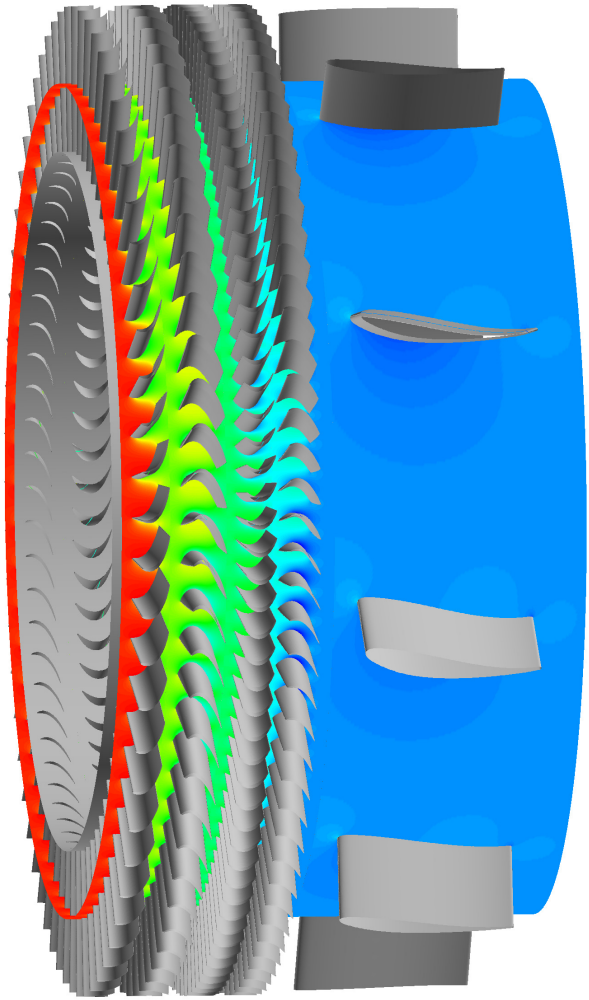

Figure 5.7: Cold-flow rig: pressure contours at mid-span (cut-back)

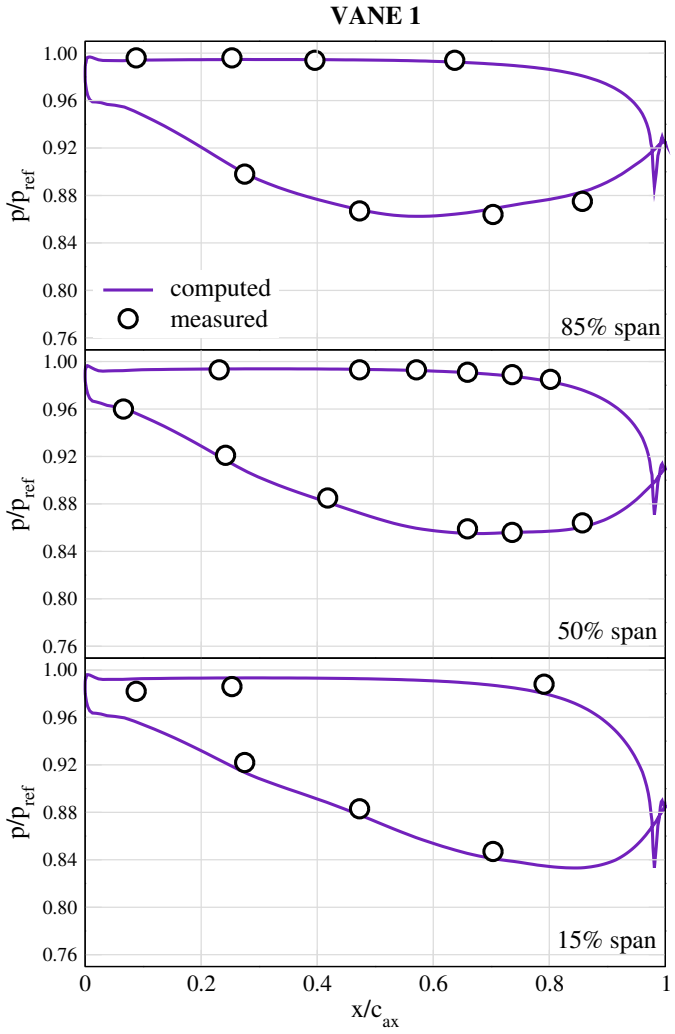

Figure 5.8: Cold-flow rig: pressure distributions on vane 1 (approach)

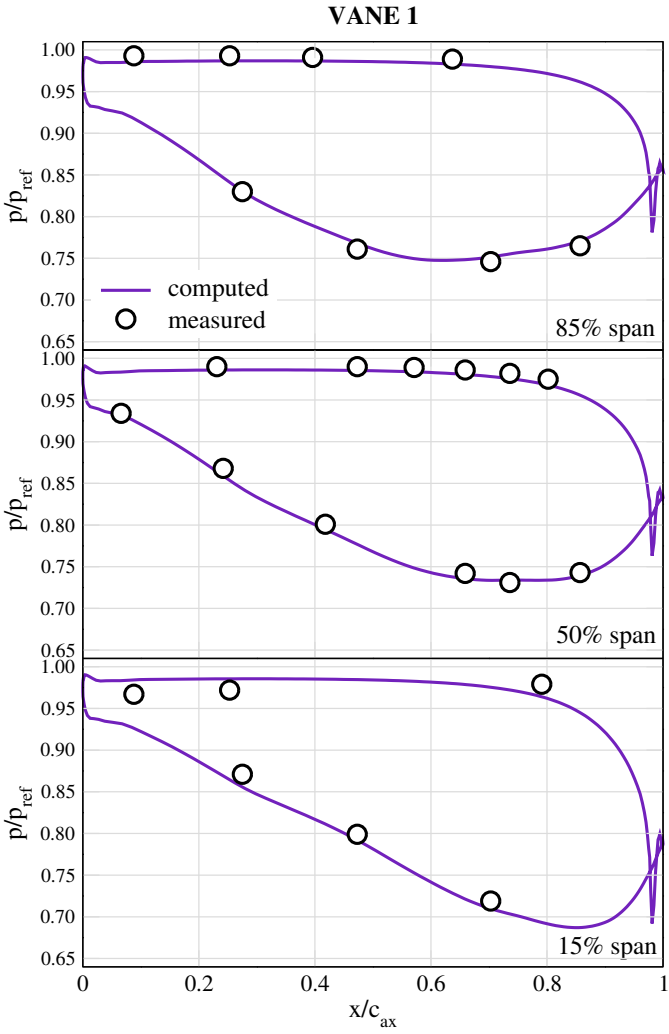

Figure 5.9: Cold-flow rig: pressure distributions on vane 1 (cutback)

5.3 Unsteady analysis of B2-TRF interaction

The validation of the 3D CAA approach described started with the unsteady analysis of the interaction between the last rotor and the turbine rear frame (TRF). Since the outlet section of the TRF is located where the radial rake of Kulite sensors are installed, the numerical results of the acoustic emissions generated by this interaction can be compared directly with the experimental data without the need of further acoustic propagations.

The acoustic database available is very large, hence it was possible to perform a comprehensive analysis of the acoustic emission of the cold flow test rig: different operating conditions along the performance curve (shown in Figure 5.4) have been simulated.

Unsteady simulations have been performed with the Traf code, taking advantage of the phase lagged boundary conditions in order to reduce the computational time. For sake of completeness, the acoustic emissions have been evaluated with the time-linearized solver Lars as well. Time-linearized computations were carried out imposing both potential and convected waves as noise sources at the TRF inlet section.

As far as the overall emissions are concerned, Figures 5.10 shows the comparison of the global emissions in terms of total PWL at the turbine exhaust for all the operating points. This results refers to the $1\times$ blade passing frequency. Overall PWL values show a very good agreement between the two CAA methods and the measurements. It can be observed that the emission trend, grows with the turbine rotational speed, as expected. Moreover the predicted values are very close to the measurements: discrepancies lie in the range of 3 dB and often in most operating points are even lower.

Results of the $2\times$ blade passing frequency have not been compares since at the operating points with higher rotational speed the frequency of the acoustic waves is higher that the

Nyquist value of the Kulite sensors.

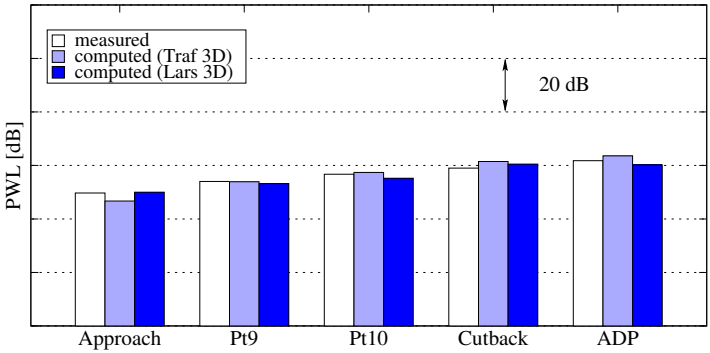

Figure 5.10: Cold-flow rig B2-TRF: total PWL at turbine exhaust (1^{st} BPF)

In sections § 5.3.1 and § 5.3.2 the acoustic results will be described more in depth, comparing the PWL values of circumferential and single modes. For sake of brevity, only the approach and cutback operating conditions will be described, being the most relevant operating points in terms of noise certification.

5.3.1 Cutback operating conditions

In Figure 5.11 on the next page the radial shapes of the most relevant modes that are present within the annular duct at cutback conditions are shown. It can be observed that the incoming perturbations interact with the TRF (which has a small number of blades), generate a large number of scattered acoustic modes, several being cut-on (highlighted in grey). This explains why turbine rear frames are a critical component from an aeroacoustic point of view and why the implementation of low-noise strategies during the design loop is so important. In the following analysis only cut-on modes

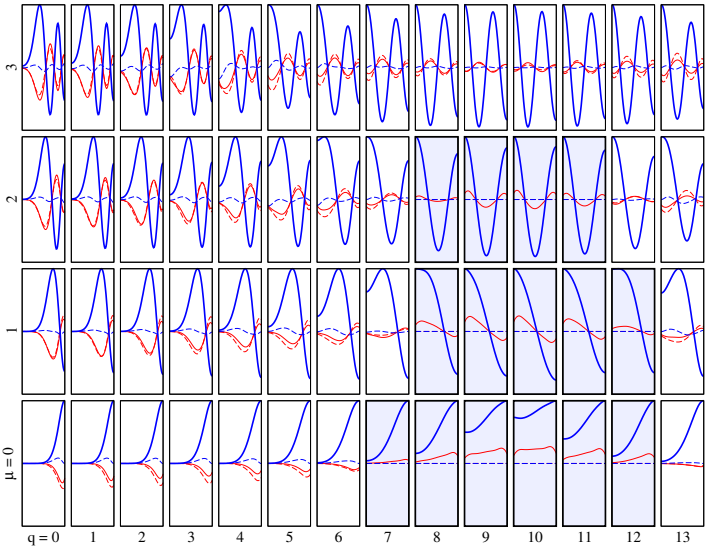

Figure 5.11: Cold-flow rig 1B2-*k*TRF: radial shape of the downstream running acoustic components (TRF exit, cut-on modes highlighted in grey)

will be analysed and compared as they turn out to be by far the most relevant at the measurements location.

Figure 5.12 on the facing page shows the acoustic results in terms of PWL split into circumferential components. Despite some small discrepancies between the numerical results and the experimental data, the tone noise emissions at the turbine exhaust are properly predicted and the general trend over the circumferential orders is consistent with the measurements. The only inconsistencies observable are in part addressed to the different methods used for the evaluation of the acoustic mode shapes: radial mode decomposition (with sheared and swirling flow) and radial modal analysis (based on Tyler-Sofrin's modes) are used to in CAA simulations and

experimental results respectively.

At the same time, the results of the two CAA methods are very close, meaning that non-linear effects have not a relevant effect for this case in tone noise generation.

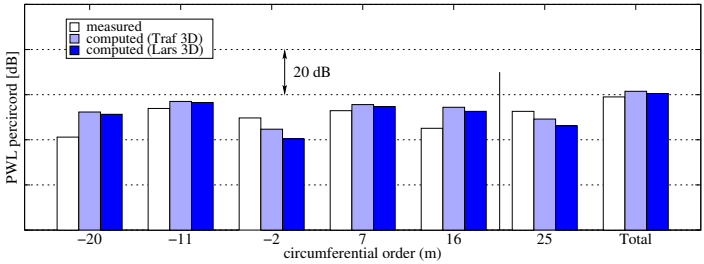

Figure 5.12: Cold-flow rig 1B2-kTRF: PWL values of the most relevant downstream running circumferential modes (TRF exit)

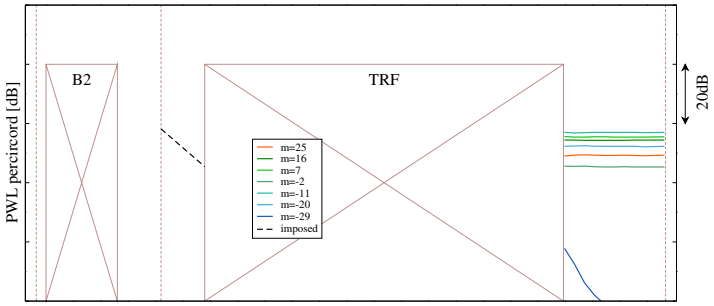

Figure 5.13: Cold-flow rig 1B2-kTRF: "spaghetti-plots" of the most relevant downstream running circumferential components in terms of PWL (non-linear CAA approach)

From the CAA simulation results it is possible to extract the evolution of each acoustic mode traveling in the inter-row

gaps as well. This is made extracting the propagating waves at different sections in the inter-row gaps. Figures 5.13 on the previous page and 5.14 show the axial evolution of the most relevant downstream running circumferential components and of the single modes respectively calculated from the non-linear method solution. It can be noticed that cut-on modes keep their acoustic power constant, while cut off modes decay with a constant decay ratio, confirming the reliability of the method and highlighting that artificial dissipation and domain discretizations do not affect the acoustic prediction.

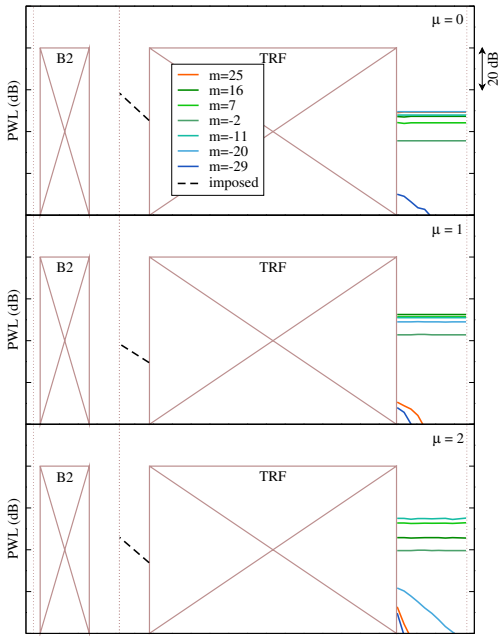

Figure 5.14: Cold-flow rig 1B2-kTRF: "spaghetti-plots" of the most relevant downstream running radial components in terms of PWL (non-linear approach)

5.3.2 Approach operating conditions

As it can be observed in Figure 5.15, at approach conditions the number of cut-on modes decreases with respect to cutback and the acoustic emissions are lower as well. This is due to the lower rotational speed and flow Mach numbers, which reduce the cut-on range (see equation 2.7).

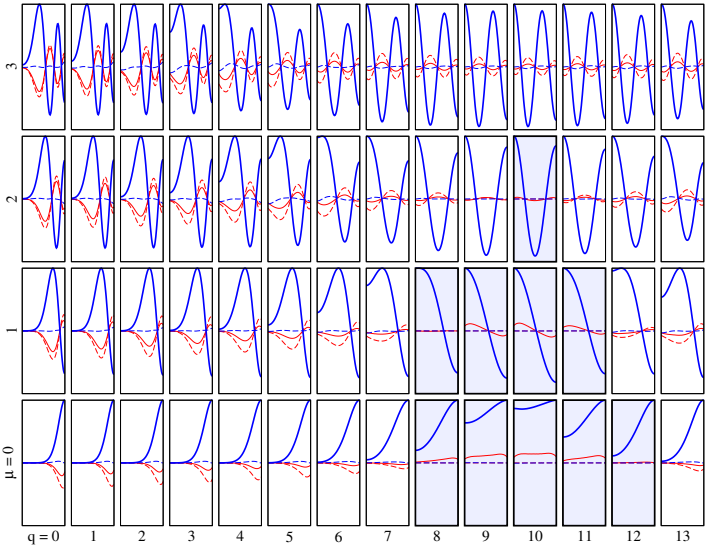

Figure 5.15: Cold-flow rig 1B2-*k*TRF: radial shape of the downstream running acoustic components (TRF exit, cut-on modes highlighted in grey)

Figure 5.16 on the next page depicts the PWL values at turbine exit split into circumferential components. Once again, the comparison between the numerical results and the measurements are pretty good: the trend has been well predicted, and the differences between the numerical values and the measurements are low.

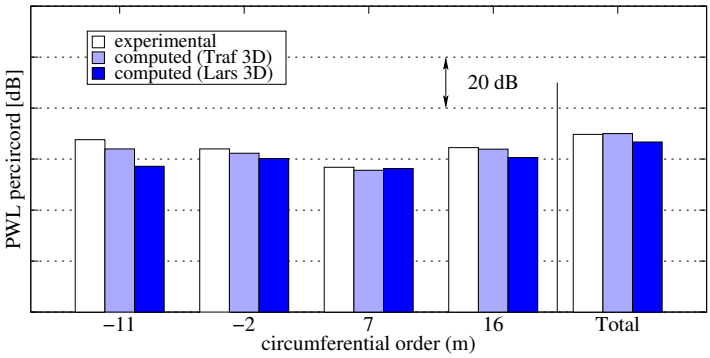

Figure 5.16: Cold-flow rig 1B2-kTRF (approach): PWL levels of the most relevant downstream running circumferential modes at the TRF exit

5.4 Acoustic assessment of V1-B1 interaction

The next step of this study consisted in the assessment of the acoustic emissions generated by the interaction between the first stator (V1) and the first rotor (B1). This analysis was performed for a different test rig configuration characterized by a radial TRF and the acoustic evaluation was limited to the two most relevant operating points in terms of noise certification: approach and cutback.

The emissions of this interaction have been simulated taking advantage of a mixed approach which exploits the non-linear CAA method (based on unsteady rotor/stator computations) to compute noise generation and the time-linearized code Lars for the following propagations. Only cut-on pressure waves have been propagated downstream up to the turbine exhaust. Simulations have been performed with the TNT procedure as well, providing a further validation for the whole procedure.

Figures 5.17(a) and 5.17(b) on the following page depict the acoustic generation and propagation history in terms of overall PWL at the exit of each row. Obviously experimental data were available only at the TRF exit where the Kulite sensors are located, hence, at the exit of previous rows, only the numerical results are shown. It can be observed that the mixed non-linear and time-linearized procedure is able to reproduce the measured values with a perfect agreement. The 2D TNT procedure, despite some major approximations intrinsically included the simplified models, is able to quickly provide very encouraging results at both operating conditions.

As already stated in the previous section, 3D CAA simulations allows more detailed analysis an a very good agreement can be observed when comparing the circumferential radial contributions to the overall acoustic emissions (see Figures 5.4 on page 93).

The axial evolution of the cut-on circumferential components from the source up to the turbine exit is depicted in Figure 5.19 on page 94. It is worth noticing how the acoustic perturbations perfectly match at the grid interfaces, meaning that all the cut-on waves are correctly propagated between adjacent domains and that there are no spurious interactions on the mesh boundaries which could have affected the reliability of the solution.

Finally, as these preliminary results match very well the measurements, this "hybrid" approach (unsteady CFD for noise generation and linearized method for noise propagation) proves to be suitable for tone noise evaluation, especially when strong rotor/stator interactions occur where the modes are generated.

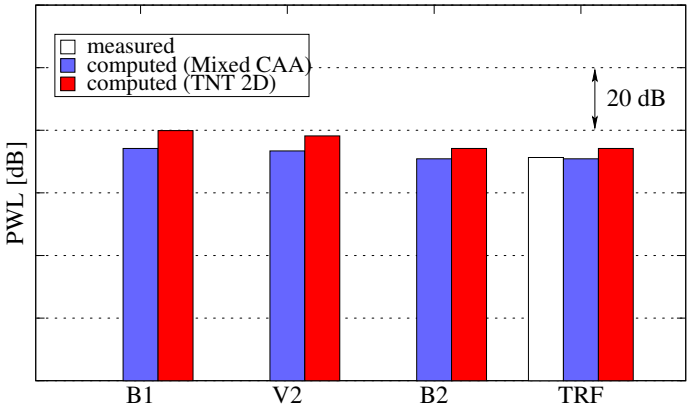

(a) Cutback

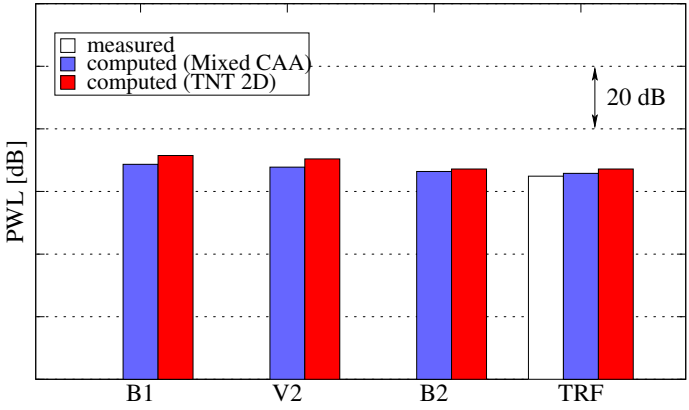

(b) Approach

Figure 5.17: Cold-flow rig 1V1-1B1: acoustic emissions at the exit of each row

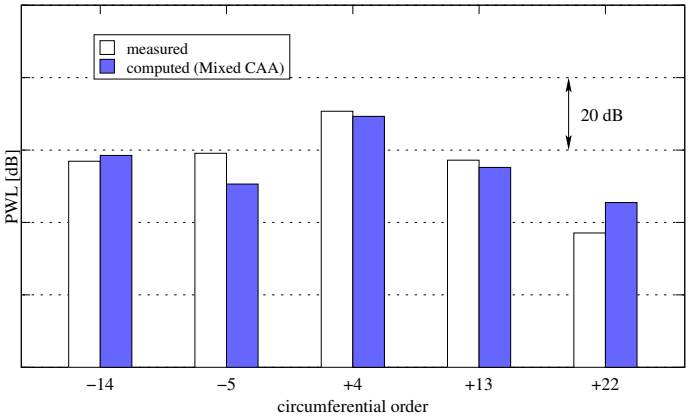

(a) Cutback

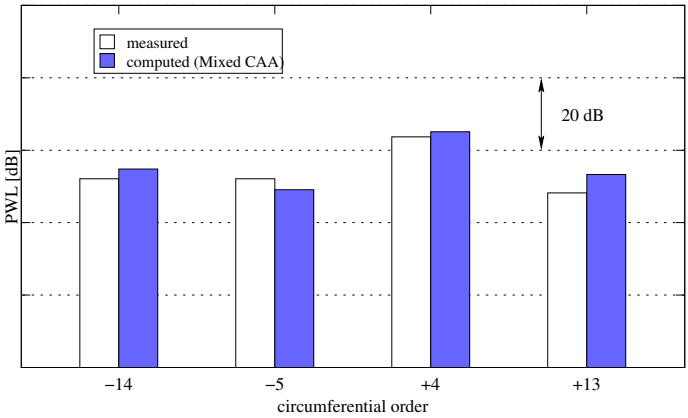

(b) Approach

Figure 5.18: Cold-flow rig 1V1-1B1: PWL values of the most relevant downstream running circumferential modes at TRF exit

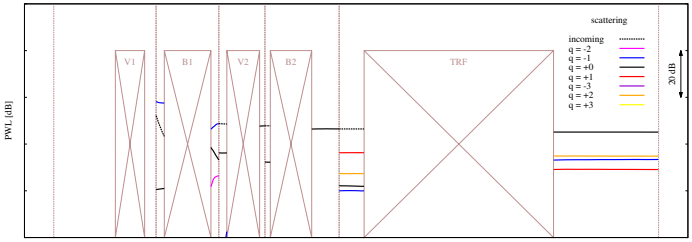

Figure 5.19: Cold-flow rig 1B2-kTRF: "spaghetti-plots" of the most relevant downstream running circumferential components in terms of PWL at approach conditions

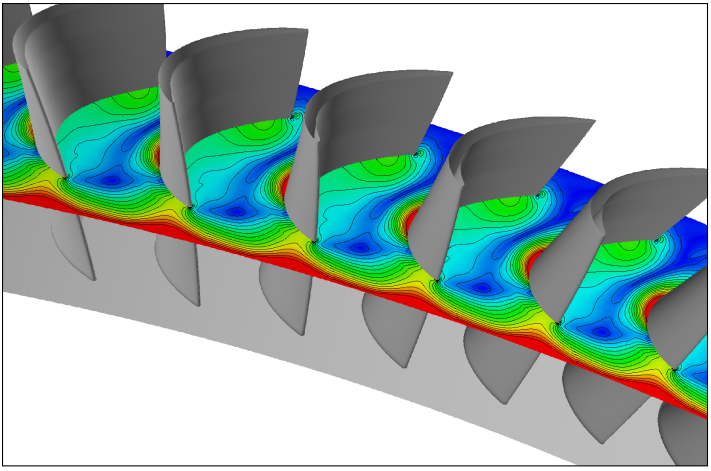

Figure 5.20: Cold-flow rig 1V1-1B1: acoustic pressure field generated by the $1 \times$ BPF of V1-B1 interaction on the first blade (non-linear CAA method, cutback)

Conclusions and further work

In this PhD thesis the problem of aeronautical noise pollution in the airport neighbourhoods has been dealt with. Since regulations on permitted acoustic emissions have become very restrictive and further tightening are expected in the next years, it is essential for commercial aircrafts to become quieter in order to keep pace with such limitations and meet the certification requirements.

Engines, in particular, generate the most relevant contribution to the overall noise at all the certification points. The investigation of the different internal sources is crucial to understand the various aeroacoustic phenomena involved in noise generation and propagation to gain deeper knowledge required to develop even more effective low-noise strategies without a detrimental effect on the overall performances (e.g. fuel consumption). To this aim, detailed experimental data are of great importance; yet under some circumstances, such as in the turbine environment, the acquisition of good acoustic data is a very challenging task due to the complex geometry and the severe operating conditions. For this reason, the interest in noise prediction methods that allowing the evaluation of the acoustic emissions before a new engine is tested with different accuracy-to-computational-time ratios has greatly increased.

In this context, the Department of Industrial Engineering

of Florence works at the development of reliable numerical tools for the prediction of low-pressure turbine tone noise. More in detail, the work described in this PhD thesis is addressed to the development of two different noise prediction methods.

For the first method, a two-dimensional model that deals with the propagation of pressure, vorticity and entropy perturbations through a blade row was implemented. This tool was the missing piece for the existing 2D noise prediction strategy and was integrated in this fast and robust procedure that is particularly suitable during the early design stages. A first validation of this model showed good prediction capabilities and it turned out to be a powerful tool to perform fast parametric analysis on the effects of primary design variables (blade counts and axial gaps, for instance).

The development of the second method makes the extraction of acoustic wave from a 3D unsteady CFD computation possible. More in detail, time-accurate CFD simulations of the rotor/stator interactions provide the tone noise generation by means of a DFT post-processing of the periodic solution. This method produces a very detailed description of both the aerodynamic and acoustic fields. Due to the large request in terms of computational time required, the use of this method is recommended during the advanced design stages.

Both tools have been applied to evaluate the acoustic emissions of a cold-flow test rig set up at the Avio facility. Acoustic measurements at the turbine exhaust are available at different operating points in order to represent the typical working conditions of aeronautical low pressure turbines. Numerical results showed a very good agreement in terms of total PWL when compared with the experimental data. The non-linear CAA method, able to account for non-linear effects, has shown a very good capability to correctly predict the circumferential and radial content of the overall emissions as well.

Finally, it is worth spending a few words about possible further developments. The two-dimensional tool already covers

all the physical phenomena concerning tone noise generation and propagation. Moreover, despite the strong approximations, it provides reliable results and hence its development can be considered closed. As far as the three-dimensional non-linear CAA procedure is concerned, next steps address these issues:

- The introduction of time-depending acoustic inlet conditions in the CFD code would allow the simulation of acoustic propagation.
- The implementation of upwind numerical schemes in order to remove the required numerical dissipation, enhancing the acoustic prediction capabilities of the code.
- The implementation of 3D non-reflecting boundary conditions at the CFD boundaries would reduce the uncertainties due to non-physical reflections at domain inlet and outlet.

Bibliography

[1] Abdol-Hamid, K., and Pao, S. P. High-end computing at nasa - Propulsion airframe aeroacousitc computational analysis. Tech. rep., National Aeronautics and Space Administration (NASA), January 2006.

[2] Aparicio, J., Serrano, A., and Vázquez, R. On the linearity of turbomachinery interaction noise. part ii: 3d analysis. *AAIA paper 2012-2309* (2012).

[3] Arnone, A. Viscous analysis of three-dimensional rotor flow using a multigrid method. *Journal of turbomachinery 116* (1994), 435–445.

[4] Arnone, A., Liou, M.-S., and Povinelli, L. Multigrid calculation of three-dimensional viscous cascade flows. *Journal of propulsion and power 9*, 4 (1993), 605–614.

[5] Arnone, A., and Pacciani, R. Rotor-stator interaction analysis using the navier-stokes equations and a multigrid method. *ASME J. Turbomach. 118*, 4 (1996), 679–689.

[6] Arnone, A., and Pacciani, R. Rotor-stator interaction analysis using the navier-stokes equations and a multigrid method. *Journal of turbomachinery 118*, 4 (October 1996), 679–689.

[7] Arnone, A., and Pacciani, R. igv-rotor interaction analysis in a transonic compressor using the navier-stokes equations. *ASME Journal of Turbomachinery 120*, 1 (1998), 143–155.

[8] Arnone, A., Pacciani, R., and Sestini, A. Multigrid computations of unsteady rotorstator interaction using the navierstokes equations. *Journal of Fluids Engineering 117* (1995), 647–652.

[9] Arnone, A., and Swanson, R. A navierstokes solver for turbomachinery applications. *ASME Journal of Turbomachinery 115*, 2 (1993), 305–313.

[10] Australian Government - Department of Infrastructure and Regional Development. *Expanding Ways to Describe and Assess Aircraft Noise* (March 2000).

[11] Baldwin, B. S., and Lomax, H. Thin layer approximation and algebraic model for separated turbulent flows. In 16^{th} *Aerospace Sciences Meeting* (Huntsville, AL, USA, January 1978). AAIA paper 78-257.

[12] Broszat, D., Kennepohl, F., Tapken, U., Moser, M., and Heitmeir, F. Validation of an acoustically 3d-designed turbine exit guide vane. In *16th AAIA/CEAS Aeroacoustic Conference (31st AAIA Aeroacoustic Conference)* (2010).

[13] Cochran, W. T., Cooley, J. W., Favin, D. L., Helms, H. D., Kaenel, R. A., Lang, W. W., Jr., G. C. M., Nelson, D. E., Rader, C. M., and Welch, P. D. What is the fast fourier transform? *Proceedings of the IEEE 55*, 10 (October 1967), 1664–1674.

[14] Cumpsty, N., and Marble, F. The interaction of entropy fluctuation with a turbine blade rows; a mechanism of turbojet engine noise. *Proc. R. Soc. Lond. A. 357* (1977), 323–344.

[15] Durán, I., and Moreau, S. Study of the attenuation of waves propagating through fixed and rotating turbine blades. In *18th AIAA/CEAS Aeroacoustics Conference (33rd AIAA Aeroacoustics Conference)* (2012).

[16] Envia, E., and Thomas, R. Recent progress in aircraft noise research. In *ARMD Technical Seminar* (October 2007).

[17] Gerolymos, G., Michon, G., and Neubauer, J. Analysis and application of chorochronic periodicity in turbomachinery rotor/stator interaction computations. *Journal of Propulsion and Power 18*, 6 (2002), 1139–1152.

[18] Giles, M. Non–reflecting boundary conditions for the euler equations. Tech. rep., MIT Dept. of Aero. and Astro., 1988. CFDL Report 88-1.

[19] Gopinath, A. K. *Efficient Fourier-based Algorithms for time-periodic unsteady problems.* PhD thesis, Stanford University, April 2007.

[20] Hanson, D. Coupled 2-dimensional cascade theory for noise and unsteady aerodynamics of blade row interaction in turbofans. Volume 1 – Theory development and parametric studies. Tech. rep., NASA Contractor Report 4506, January 1994.

[21] Haselbach, F., Schiffer, H. P., Horsman, M., Dressen, S., Harvey, N., and Read, S. The application of ultra high lift blading in the br715 lp turbine. *Journal of Turbomachinery 124*, 1 (2002), 45–51.

[22] Howell, R. J., Ramesh, O. N., Hodson, H. P., Harvey, N., and Schulte, V. High lift and aft-loaded profiles for low-pressure turbines. *Journal of Turbomachinery 123*, 1 (2001), 181–188.

[23] Huff, D. Noise reduction technologies for turbofan engines. Tech. rep., NASA/TM–2007-214495, September 2007.

[24] International Civil Aviation Organization (ICAO). *Environmental Protection vol. 1 Aircraft Noise* (July 2008).

[25] Jameson, A. Numerical solution of the euler equations for compressible inviscid fluids. In *Numerical Methods for the Euler Equations of Fluid Dynamics* (1985), F. A. et al., Ed., SIAM, pp. 199–245.

[26] Jameson, A. Time dependent calculations using multigrid with applications to unsteady flows past airfoils and wings. In 10^{th} *AIAA Computational Fluid Dynamics Conference* (June 1991).

[27] Jameson, A., Schmidt, W., and Turkel, E. Numerical solutions of the euler equations by finite volume methods using rungekutta timestepping schemes. In 14^{th} *Fluid and Plasma Dynamics Conference* (June 1981).

[28] Marble, F., and Candle, S. Acoustic disturbance from gas non-uniformities convected through a nozzle. *Journal of sound and vibration 55* (1977).

[29] Martinelli, L., and Jameson, A. Validation of a multigrid method for reynolds averaged equations. *AIAA paper 88–0414* (1988). AIAA 26^{th} Aerospace Sciences Meeting, January, Reno, NV.

[30] Menter, F. R. Twoequations eddy viscosity turbulence models for engineering applications. *AAIA J. 32*, 8 (1994), 1598–1605.

[31] Montgomery, M., and Verdon, J. A three-dimensional linearized unsteady Euler analysis for turbomachinery blade rows. Tech. rep., NASA Contractor Report 4770, March 1997.

[32] Myers, M. Transport of energy by disturbances in arbitrary steady flow. *Journal of Fluid Mechanics 226* (1991), 383–400.

[33] Pinelli, L. *Development of a computational method for turbomachinery tone noise analysis.* Energy engineering PhD thesis, University of Florence, Italy, December 2010.

[34] Pinelli, L., Poli, F., Di Grazia, E., Arnone, A., and Torzo, D. A comprehensive numerical study of tone noise emissions in a multistage cold flow rig. In *19th AAIA/CEAS Aeroacoustics Conference (34th AIAA Aeroacoustics Conference)* (2013).

[35] Pinelli, L., Poli, F., Marconcini, M., Arnone, A., Spano, E., and Torzo, D. Validation of a 3d linearized method for turbomachinery tone noise analysis. In *IGTI ASME Turbo Expo* (2011). ASME paper GT2011-45886.

[36] Pinelli, L., Poli, F., Marconcini, M., Arnone, A., Spano, E., Torzo, D., and Schipani, C. A linearized method for tone noise generation and propagation analysis in a multistage contra-rotating turbine. In 9^{th} *European Conference on Turbomachinery Fluid Dynamics and Thermodynamics* (2011).

[37] Pinelli, L., Torzo, D., Poli, F., and Arnone, A. Assessment of numerical methods for low pressure turbine tone noise prediction. In 10^{th} *European Conference on Turbomachinery Fluid Dynamics and Thermodynamics* (2013).

[38] Poli, F., Arnone, A., and Schipani, C. A 3D linearized method for turbomachinery tone noise analysis with 3D non-reflecting boundary conditions. In 8^{th} *European Conference on Turbomachinery Fluid Dynamics and Thermodynamics* (2009).

[39] Reed, D., Herkes, W., and Shivanshankara, B. The boeing quiet technology demonstrator program. In

25th ICAS International Congress of the Aeronautical Sciences (2006).

[40] Rife, D. C., and Vincent, G. A. Use of the discrete fouries transform in the measurements of frequencies and levels of tones. *The bell system technical journal 49* (February 1970), 197–228.

[41] Smith, N. Discrete frequency sound generation in axial flow turbomachines. Tech. rep., 1973. Report R. & M. n^{o} 3709.

[42] Spalart, P. R., and Allmaras, S. R. A one-equation turbulence model for aerodynamic flows. *La Recherche Aérospatiale 1* (1994), 5–21.

[43] Spalart, P. R., and Shur, M. On the sensitization of turbulence models to rotation and curvature. *Aerosp. Sci. Technol. 1*, 5 (1997), 297–302.

[44] Sugimoto, R., Astley, J., and Murray, P. Low frequency liners for turbofan engines. 20th International Congress on Acoustics, ICA 2010.

[45] Swanson, R., and Turkel, E. Artificial dissipation and central difference schemes for the euler and navier–stokes equations. *AIAA paper 87–1107–CP* (1987). 8^{th} Computational Fluid Dynamics Conference, June 9–11, Honolulu, HI, USA.

[46] Taddei, F., Cinelli, C., Lucia, M. D., and Schipani, C. Experimental investigation of low pressure turbine noise: Radial mode analysis for swirling flows. In 12^{th} *International Symposium on Unsteady Aerodynamics, Aeroacoustics and Aeroelasticity of Turbomachines* (2009).

[47] Turkel, E. Improving the accuracy of central difference schemes. Tech. rep., ICASE 88-53, 1988.

[48] Tyler, J., and Sofrin, T. Axial flow compressor noise studies. *Trans. Society of Automotive Engineers 70* (1962), 309–332.

[49] Verdon, J., Montgomery, M., and Chuang, H. Development of a linearized unsteady Euler analysis with application to wake/blade-row interactions. Tech. rep., NASA Contractor Report 208879, 1999.

[50] Weckmüller, C., Guérin, S., and Ashcroft, G. Cfd-caa coupling applied to dlr uhbr-fan: Comparison to experimental data. In 15^{th} *AAIA/CEAS Aeroacoustic Conference (*30^{th} *AAIA Aeroacoustics Conference)* (2009).

[51] Wilcox, D. C. *Turbulence Modeling for CFD*, 2^{nd} ed. DCW Ind. Inc., La Cañada, CA, USA, 1998.

[52] Wilcox, D. C. Formulation of the $k-\omega$ turbulence model revisited. *AAIA J. 46*, 11 (2008), 2823–2838.

[53] Wilson, A. *A Method for Deriving Tone Noise Information from CFD Calculations on the Aeroengine Fan Stage*. Defense Technical Information Center, 2001.

[54] Zante, D. V., and Envia, E. Simulation of turbine tone noise generation using a turbomachinery aerodynamics solver. In 15^{th} *AAIA/CEAS Aeroacoustic Conference (*30^{th} *AAIA Aeroacoustics Conference)* (2009).